Nonrecursive Control for Formation-Containment of HFV Swarms With Dynamic Event-Triggered Communication

Lv, Maolong; De Schutter, B.H.K.; Baldi, S.

DOI
10.1109/TII.2022.3163573

Publication date
2023

Document Version
Final published version

Published in
IEEE Transactions on Industrial Informatics

Nonrecursive Control for Formation-Containment of HFV Swarms With Dynamic Event-Triggered Communication

Maolong Lv, Bart De Schutter, *Fellow, IEEE*, and Simone Baldi, *Senior Member, IEEE*

***Abstract*—This article proposes an output-feedback control protocol for hypersonic flight vehicle (HFV) swarms considering dynamic event-triggered communication. The peculiarities of the proposed method over existing ones consist in the following: 1) While carrying out scheduled maneuvers, the outputs of follower HFVs converge inside the convex hull spanned by leader HFVs whose task is to maintain a geometric space configuration; 2) a simple nonrecursive output-feedback design is established without involving any intermediate control laws or requiring full-state information; 3) an error-dependent monotonically decreasing exponential term is incorporated into the dynamic event-triggered threshold to reduce the communication bandwidth while preserving the desired track performance and excluding Zeno behavior. Comparative simulation results validate the effectiveness of the proposed methodology.**

***Index Terms*—Event-triggered communication, formation-containment control, hypersonic flight vehicles (HFVs).**

I. Introduction

OVER the past decades, several studies have been carried out on hypersonic flight vehicles (HFVs) [1], [2] and formations of HFVs [3]–[5]. Sliding mode control [6], [7], backstepping [8]–[10], dynamic surface control [11], and command-filtered backstepping [12] have been proved to handle various model uncertainties in HFVs. On the other hand, these methods require a recursive design procedure that inevitably suffers from repeated differentiation of intermediate control laws and a heavy computational burden [13]. Besides, the aforementioned methods [6]–[12] are solely suited for a single HFV and fail to realize more complex flight missions such as formation control, containment control, and their combinations [14]–[18].

Cooperative control protocols proposed in the literature [3]–[5], [14]–[18] rely on continuous or periodic information exchange among HFVs. To be precise, the entire state information of each HFV must be broadcast to neighboring HFVs. This inevitably poses high pressure on network resources and the limited communication bandwidth, especially when the number of HFVs grows [19]. Event-triggered communication has been proposed to handle such issues, in the sense that information transmission among multiple vehicles occurs only when some error-dependent function exceeds a certain threshold [20]–[27]. Again, the aforesaid approaches either adopt a recursive design procedure or rely on full-state information, which is unrealistic for HFVs due to the complicated plant characteristics and drastic variation of flight conditions in hypersonic flight [1], [7]. In the absence of full-state information, although observers have been proposed in [28] and [29], it is a crucial and still unexplored topic to make the observer convergence rate independent on the initial conditions of HFVs and to embed this convergence notion in event-triggered formation control for HFV swarms.

Motivated by above discussions, the main contributions of this article are threefold.

1) Unlike the protocols designed for single-leader HFV swarms [3]–[5], a formation-containment control protocol is developed for HFV swarms with multiple leader HFVs such that the follower HFVs converge to the convex hull spanned by leader HFVs, while the leader HFVs maintain a geometric space configuration.
2) Different from recursive design methods [6]–[12], we propose a nonrecursive output-feedback design framework for HFVs which does not involve any intermediate control laws. This is achieved by showing that the HFV dynamics can be written in a special cascaded form.
3) Compared with the existing event-triggered mechanisms [20]–[27], a new error-dependent monotonically decreasing exponential term is delicately embedded into

Manuscript received 14 February 2022; accepted 23 March 2022. Date of publication 30 March 2022; date of current version 3 March 2023. This work was supported in part by the "Young Talent Fund of China Association for Science and Technology in Shaanxi, China," in part by the Research Fund for International Scientists under Grant 62150610499, in part by the Natural Science Foundation of China under Grants 62073074 and 62003252, in part by the Special Funding for Overseas under Grant 6207011901, and in part by Double Innovation Plan under Grant 4207012004. Paper no. TII-22-0717. (*Corresponding author: Simone Baldi.*)

Maolong Lv is with the Air Traffic Control and Navigation College, Air Force Engineering University, Xi'an 710051, China, and also with the College of Aeronautics Engineering, Air Force Engineering University, Xi'an 710038, China (e-mail: maolonglv@163.com).

Bart De Schutter is with the Delft Center for Systems and Control, Delft University of Technology TU Delft, 2628 CD Delft, The Netherlands (e-mail: b.deschutter@tudelft.nl).

Simone Baldi is with the School of Mathematics, Southeast University, Nanjing 210096, China, and also with the Delft Center for Systems and Control, Delft University of Technology TU Delft, 2628 CD Delft, The Netherlands (e-mail: s.baldi@tudelft.nl).

Color versions of one or more figures in this article are available at https://doi.org/10.1109/TII.2022.3163573.

Digital Object Identifier 10.1109/TII.2022.3163573

the dynamic triggering threshold for the purpose of reducing the frequency of data transmission among HFVs, while guaranteeing desired tracking accuracy and excluding Zeno behavior.

Notations: Throughout this article, $\mathbb{R}$ and $\mathbb{N}^+$ stand for the sets of real numbers and positive integers, respectively, $\otimes$ is the Kronecker product, $f^{(i)}(t)$ denotes the i-order derivative of a function $f(t)$, $\boldsymbol{I}_n$ is the identity matrix in the space $\mathbb{R}^{n\times n}$, $\boldsymbol{0}_{1\times n}$ stands for a $1\times n$ zero matrix, $\underline{\boldsymbol{1}}_p$ denotes the $p\times 1$ vector of all ones, for a vector $\boldsymbol{A}=[A_1,\ldots,A_N]^\top$, $\lceil\boldsymbol{A}\rfloor^l=[|A_1|^l\mathrm{sgn}(A_1),\ldots,|A_N|^l\mathrm{sgn}(A_N)]^\top$, $||\boldsymbol{A}||$ denotes the Euclidean norm, and for a matrix $\boldsymbol{Q}$, $\boldsymbol{Q}>0$ denotes that $\boldsymbol{Q}$ is a positive definite matrix, and $\sigma_{\min}(\boldsymbol{Q})$ and $\sigma_{\max}(\boldsymbol{Q})$ are the minimum and maximum eigenvalues of $\boldsymbol{Q}$, respectively.

II. Vehicle Model and Problem Formulation

A. Hypersonic Flight Vehicle Dynamics

Consider a HFV swarm system composed of N followers and M leaders. Similar to [30], the longitudinal dynamics of the ith HFV are described by a set of differential equations for rigid-body states $[h_i,\gamma_i,\alpha_i,q_i,x_i,V_i]^\top$ and flexible states $\boldsymbol{\eta}_i=[\eta_{i,1},\dot\eta_{i,1},\ldots,\eta_{i,n},\dot\eta_{i.n}]^\top$, $n\in\mathbb{N}^+$

$$\begin{aligned}
&\dot h_i=V_i\sin\gamma_i,\quad \dot\gamma_i=\frac{L_i+T_i\sin\alpha_i}{m_iV_i}-\frac{g_i\cos\gamma_i}{V_i},\\
&\dot\alpha_i=q_i-\frac{L_i+T_i\sin\alpha_i}{m_iV_i}+\frac{g_i\cos\gamma_i}{V_i},\quad \dot q_i=\frac{M_i}{I_i^{yy}},\\
&\dot x_i=V_i\cos\gamma_i,\quad \dot V_i=\frac{T_i\cos\alpha_i-D_i}{m_i}-g_i\sin\gamma_i,\\
&\ddot\eta_{i,j}=-2\zeta_{i,j}\omega_{i,j}\dot\eta_{i,j}-\omega_{i,j}^2\eta_{i,j}+N_{i,j},\quad j=1,\ldots,n \qquad (1)
\end{aligned}$$

for $i\in F\bigcup L$, where $F=\{1,2,\ldots,N\}$ and $L=\{N+1,\ldots,N+M\}$ represent the follower and leader sets, respectively; h_i and x_i are the vertical position (altitude) and the forward position with respect to the z- and x- directions of the earth-fixed reference frame; γ_i, α_i, q_i, and V_i are the flight path angle, angle of attack, pitch rate, and velocity; $\boldsymbol{\eta}_i$ denotes the amplitude of the ith bending mode of the fuselage, which is modeled as a single flexible structure with mass-normalized mode shapes; m_i, I_i^{yy}, g_i, $\zeta_{i,j}$, and $\omega_{i,j}$ represent the vehicle mass, moment of inertia, gravitational acceleration, damping ratio, and flexible mode frequency; $N_{i,j}$, L_i, D_i, T_i, and M_i denote the generalized elastic forces, lift, drag, thrust, and pitching moment, given as follows:

$$\begin{aligned}
L_i=&\ \bar q_iS_iC_i^L\left(\alpha_i,\delta_i^{\mathrm{e}},\delta_i^{\mathrm{c}},\boldsymbol{\eta}_i\right),\\
D_i=&\ \bar q_iS_iC_i^D\left(\alpha_i,\delta_i^{\mathrm{e}},\delta_i^{\mathrm{c}},\boldsymbol{\eta}_i\right),\\
T_i=&\ \bar q_iS_i\left[C_i^{T,\Phi}\left(\alpha_i\right)\Phi_i+C_i^T\left(\alpha_i\right)+\boldsymbol{C}_i^{T,\boldsymbol{\eta}_i}\boldsymbol{\eta}_i\right],\\
M_i=&\ z_i^TT_i+\bar q_iS_i\bar c_iC_i^M\left(\alpha_i,\delta_i^{\mathrm{e}},\delta_i^{\mathrm{c}},\boldsymbol{\eta}_i\right),\\
N_{i,j}=&\ \bar q_iS_i\left[N_{i,j}^{\alpha_i^2}\alpha_i^2+N_{i,j}^{\alpha_i}\alpha_i+N_{i,j}^{\delta_i^{\mathrm{e}}}\delta_i^{\mathrm{e}}+N_{i,j}^{\delta_i^{\mathrm{c}}}\delta_i^{\mathrm{c}}\right.\\
&\left.+N_{i,j}^0+\boldsymbol{N}_{i,j}^{\boldsymbol{\eta}_i}\boldsymbol{\eta}_i\right],\ j=1,\ldots,n \qquad (2)
\end{aligned}$$

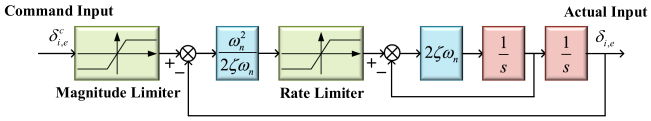

Fig. 1. Filter that generates magnitude, bandwidth, and rate constraints.

where $\bar q_i$, S_i, z_i^T, and $\bar c_i$ denote the dynamic pressure, reference area, thrust moment arm, and reference length. The control inputs of the HFV are Φ_i, δ_i^{e}, and δ_i^{c}, representing the fuel equivalence ratio, deflection of the elevator, and deflection of the canard. The coefficient of the functions in (2) are modeled via curve-fitting as [11]

$$\begin{aligned}
C_i^T=&\sum_{k=1}^{3}C_i^{T,\alpha_i^k}\alpha_i^k+C_i^{T,0},C_i^{T,\Phi}=\sum_{k=1}^{3}C_i^{T,\Phi,\alpha_i^k}\alpha_i^k+C_i^{T,\Phi,0},\\
C_i^M=&\sum_{k=1}^{2}C_i^{M,\alpha_i^k}\alpha_i^k+C_i^{M,\delta_i^{\mathrm{e}}}\delta_i^{\mathrm{e}}+C_i^{M,\delta_i^{\mathrm{c}}}\delta_i^{\mathrm{c}}+C_i^{M,0}+\boldsymbol{C}_i^{M,\boldsymbol{\eta}_i}\boldsymbol{\eta}_i,\\
C_i^L=&C_i^{L,\alpha_i}\alpha_i+C_i^{L,\delta_i^{\mathrm{e}}}\delta_i^{\mathrm{e}}+C_i^{L,\delta_i^{\mathrm{c}}}\delta_i^{\mathrm{c}}+C_i^{L,0}+\boldsymbol{C}_i^{L,\boldsymbol{\eta}_i}\boldsymbol{\eta}_i,\\
C_i^D=&C_i^{D,\alpha_i^2}\alpha_i^2+C_i^{D,\alpha_i}\alpha_i+C_i^{D,\delta_i^{\mathrm{e}2}}\delta_i^{\mathrm{e}2}+C_i^{D,\delta_i^{\mathrm{e}}}\delta_i^{\mathrm{e}}\\
&+C_i^{D,\delta_i^{\mathrm{c}2}}\delta_i^{\mathrm{c}2}+C_i^{D,\delta_i^{\mathrm{c}}}\delta_i^{\mathrm{c}}+C_i^{D,0}+\boldsymbol{C}_i^{D,\boldsymbol{\eta}_i}\boldsymbol{\eta}_i,\\
\boldsymbol{C}_{i,j}^{\boldsymbol{\eta}_i}=&\left[C_{i,j}^{\eta_{i,1}},0,\ldots,C_{i,j}^{\eta_{i,n}},0\right],\ j=T,M,L,D,\\
\boldsymbol{N}_{i,l}^{\boldsymbol{\eta}_i}=&\left[N_{i,l}^{\eta_{i,1}},0,\ldots,N_{i,l}^{\eta_{i,n}},0\right],\ l=1,\ldots,n. \qquad (3)
\end{aligned}$$

To cancel the lift-elevator coupling, δ_i^{c} is ganged with δ_i^{e}, i.e., $\delta_i^{\mathrm{c}}=k_i^{\mathrm{e,c}}\delta_i^{\mathrm{e}}$, $k_i^{\mathrm{e,c}}=-C_i^{L,\delta_i^{\mathrm{e}}}/C_i^{L,\delta_i^{\mathrm{c}}}$ [29]. Thus, the control inputs become Φ_i and δ_i^{e}. The deflection of the elevator δ_i^{e} is adjusted through the electric actuator. The electric actuator dynamics can be well approximated as the following second-order dynamics for control system design [11]:

$$\ddot\delta_i^{\mathrm{e}}=-2\zeta\omega_{\mathrm{n}}\dot\delta_i^{\mathrm{e}}-\omega_{\mathrm{n}}^2\delta_i^{\mathrm{e}}+\omega_{\mathrm{n}}^2\delta_i^{\mathrm{e,c}} \qquad (4)$$

where ω_{n} is the undamped natural frequency and ζ is the damping ratio. Further, considering practical magnitude, bandwidth, and rate constraints, the input signal δ_i^{e} is eventually obtained by the command $\delta_i^{\mathrm{e,c}}$ filtered through a linear, stable, and low-pass command filter (as shown in Fig. 1). Similarly, the input signal Φ_i is obtained by the command Φ_i^{c} filtered through a command filter similar to that in Fig. 1.

B. Model Decomposition

The longitudinal dynamics (1) can be divided into vertical dynamics $[h_i,\gamma_i,\alpha_i,q_i]^\top$ and forward dynamics $[x_i,V_i]^\top$. In addition, the following approximations are standard in the literature: The flight path angle γ_i is small during the cruise phase so that $\sin\gamma_i\approx\gamma_i$ [29]; the angle of attack α_i is sufficiently small so that the term $T_i\sin\alpha_i$ is far smaller than the lift L_i and can be neglected [11]. Accordingly, the vertical dynamics can

be rewritten as

$$\begin{cases} \dot{h}_i = V_i\gamma_i + d_{i,1}, \\ \dot{\gamma}_i = \boldsymbol{\Theta}_{i,2}^{\top}(\boldsymbol{f}_{i,2} + \boldsymbol{g}_{i,2}\alpha_i) + d_{i,2}, \\ \dot{\alpha}_i = \boldsymbol{\Theta}_{i,3}^{\top}(\boldsymbol{f}_{i,3} + \boldsymbol{g}_{i,3}q_i) + d_{i,3}, \\ \dot{q}_i = \boldsymbol{\Theta}_{i,4}^{\top}(\boldsymbol{f}_{i,4} + \boldsymbol{g}_{i,4}\delta_i^{\mathrm{e}}) + d_{i,4} \end{cases} \tag{5}$$

where $\boldsymbol{\Theta}_{i,2} = [\frac{S_i}{m_i}C_i^{L,\alpha_i}, \frac{S_i}{m_i}C_i^{L,0}, 1]^{\top}$, $\boldsymbol{\Theta}_{i,3} = [1, \frac{S_i}{m_i}C_i^{L,\alpha_i}, \frac{S_i}{m_i}C_i^{L,0}, 1]^{\top}$, $\boldsymbol{\Theta}_{i,4} = \frac{S_i}{I_i^{yy}}[\bar{c}_iC_i^{M,\delta_i^{\mathrm{e}}}, \bar{c}_ik_i^{\mathrm{e,c}}C_i^{M,\delta_i^{\mathrm{c}}}, z_i^TC_i^{T,\Phi,\alpha_i^3}, z_i^TC_i^{T,\Phi,\alpha_i^2}, z_i^TC_i^{T,\Phi,\alpha_i}, z_i^TC_i^{T,\Phi,0}, z_i^TC_i^{T,\alpha_i^3}, (z_i^TC_i^{T,\alpha_i^2} + \bar{c}_iC_i^{M,\alpha_i^2}), (z_i^TC_i^{T,\alpha_i} + \bar{c}_iC_i^{M,\alpha_i}), (z_i^TC_i^{T,0} + \bar{c}_iC_i^{M,0})]^{\top}$, $\boldsymbol{g}_{i,2} = [\frac{\bar{q}_i}{V_i}, \boldsymbol{0}_{1\times 2}]^{\top}$, $\boldsymbol{g}_{i,3} = [1, \boldsymbol{0}_{1\times 3}]^{\top}$, $\boldsymbol{g}_{i,4} = [\bar{q}_i, \bar{q}_i, \boldsymbol{0}_{1\times 8}]^{\top}$, $\boldsymbol{f}_{i,2} = [0, \frac{\bar{q}_i}{V_i}, -\frac{g_i}{V_i}\cos\gamma_i]^{\top}$, $\boldsymbol{f}_{i,3} = \frac{\bar{q}_i}{V_i}[0, -\alpha_i, -1, \frac{g_i}{\bar{q}_i}\cos\gamma_i]^{\top}$, and $\boldsymbol{f}_{i,4} = \bar{q}_i[\boldsymbol{0}_{1\times 2}, \alpha_i^3\Phi_i, \alpha_i^2\Phi_i, \alpha_i\Phi_i, \Phi_i, \alpha_i^3, \alpha_i^2, \alpha_i, 1]^{\top}$. The lumped disturbances $d_{i,j}$, $j = 1, \ldots, 4$ brought by external disturbances such as gust, turbulence, and atmospheric disturbances, as well as structural flexibility from the aerothermoelastic effects, can be expressed as $d_{i,1} = \Delta_{i,1}$, $d_{i,2} = \frac{\bar{q}_iS_i}{m_iV_i}\boldsymbol{C}_i^{L,\boldsymbol{\eta}_i}\boldsymbol{\eta}_i + \Delta_{i,2}$, $d_{i,3} = -\frac{\bar{q}_iS_i}{m_iV_i}\boldsymbol{C}_i^{L,\boldsymbol{\eta}_i}\boldsymbol{\eta}_i + \Delta_{i,3}$, and $d_{i,4} = \frac{z_i^T\bar{q}_iS_i}{I_i^{yy}}\boldsymbol{C}_i^{T,\boldsymbol{\eta}_i}\boldsymbol{\eta}_i + \frac{\bar{q}_iS_i\bar{c}_i}{I_i^{yy}}\boldsymbol{C}_i^{M,\boldsymbol{\eta}_i}\boldsymbol{\eta}_i + \Delta_{i,4}$, with $\Delta_{i,j}$, $j = 1, \ldots, 4$ representing the external disturbances in vertical dynamics. The forward dynamics can be rewritten as

$$\begin{cases} \dot{x}_i = V_i\cos\gamma_i + d_{i,5}, \\ \dot{V}_i = \boldsymbol{\Theta}_{i,6}^{\top}(\boldsymbol{f}_{i,6} + \boldsymbol{g}_{i,6}\Phi_i) + d_{i,6} \end{cases} \tag{6}$$

where $\boldsymbol{\Theta}_{i,6} = \frac{S_i}{m_i}[C_i^{T,\Phi,\alpha_i^3}, C_i^{T,\Phi_i,\alpha_i^2}, C_i^{T,\Phi,\alpha_i}, C_i^{T,\Phi,0}, C_i^{T,\alpha_i^3}, C_i^{T,\alpha_i^2}, C_i^{T,\alpha_i}, C_i^{T,0}, C_i^{D,\alpha_i^2}, C_i^{D,\alpha_i}, (C_i^{D,\delta_i^{\mathrm{e}2}} + k_i^{\mathrm{e,c}2}C_i^{D,\delta_i^{\mathrm{c}2}}), (C_i^{D,\delta_i^{\mathrm{e}}} + k_i^{\mathrm{e,c}}C_i^{D,\delta_i^{\mathrm{c}}}), C_i^{D,0}, \frac{m_i}{S_i}]^{\top}$, $\boldsymbol{g}_{i,5} = \bar{q}_i\cos\alpha_i[\alpha_i^3, \alpha_i^2, \alpha_i, 1, \boldsymbol{0}_{1\times 10}]^{\top}$, and $\boldsymbol{f}_{i,5} = \bar{q}_i[\boldsymbol{0}_{1\times 4}, \alpha_i^3\cos\alpha_i, \alpha_i^2\cos\alpha_i, \alpha_i\cos\alpha_i, \cos\alpha_i, -\alpha_i^2, -\alpha_i, -\delta_i^{\mathrm{e}2}, -\delta_i^{\mathrm{e}}, -1, -\frac{g_i}{\bar{q}_i}\sin\gamma_i]^{\top}$. The lumped disturbances are $d_{i,5} = \Delta_{i,5}$ and $d_{i,6} = \frac{\bar{q}_iS_i}{m_i}\boldsymbol{C}_i^{T,\boldsymbol{\eta}_i}\boldsymbol{\eta}_i\cos\alpha_i - \frac{\bar{q}_iS_i}{m_i}\boldsymbol{C}_i^{D,\boldsymbol{\eta}_i}\boldsymbol{\eta}_i + \Delta_{i,6}$ with $\Delta_{i,5}$ and $\Delta_{i,6}$ denoting the external disturbances in forward dynamics.

C. Basic Graph Theory

The information transmission among HFVs is represented by a directed graph $\mathcal{G} \triangleq (\mathcal{V}, \mathcal{E})$, where $\mathcal{V} = \{1, \ldots, N+M\}$ denotes the set of vertices corresponding to N follower HFVs and M leader HFVs. The connectivity matrix $\boldsymbol{\mathcal{A}} = [a_{ij}] \in \mathbb{R}^{(N+M)\times(N+M)}$, in-degree matrix $\boldsymbol{\mathcal{D}} = \mathrm{diag}[\mathcal{D}_i] \in \mathbb{R}^{(N+M)\times(N+M)}$, Laplacian matrix $\boldsymbol{\mathcal{L}} = \boldsymbol{\mathcal{D}} - \boldsymbol{\mathcal{A}} = \begin{bmatrix} \boldsymbol{\mathcal{L}}_1 & \boldsymbol{\mathcal{L}}_2 \\ \boldsymbol{0}_{M\times N} & \boldsymbol{0}_{M\times M} \end{bmatrix}$, and set of neighbors for the ith HFV $\mathcal{N}_i$ are defined similarly to [17], where $\boldsymbol{\mathcal{L}}_1 \in \mathbb{R}^{N\times N}$ is the matrix related to the information flow among N follower HFVs and $\boldsymbol{\mathcal{L}}_2 \in \mathbb{R}^{N\times M}$ is the matrix associated with the information flow from leader HFVs to follower HFVs. The information transmission among N follower HFVs is represented by the directed graph $\mathcal{G}_{\dashv} \triangleq (\mathcal{V}_{\dashv}, \mathcal{E}_{\dashv})$ which is a subgraph of $\mathcal{G}$ with Laplacian matrix $\boldsymbol{\mathcal{L}}_{\dashv}$ and a set of neighbors for the ith follower HFV $\mathcal{N}_{\dashv}^i$.

To guarantee the connectivity of $\mathcal{G}$, we assume that for each follower HFV, there exists at least one leader HFV that has a path to the follower HFV. Based on this, we can conclude that $\boldsymbol{\mathcal{L}}_1$ is positive definite, each entry of $-\boldsymbol{\mathcal{L}}_1^{-1}\boldsymbol{\mathcal{L}}_2$ is nonnegative, and each row sum of $-\boldsymbol{\mathcal{L}}_1^{-1}\boldsymbol{\mathcal{L}}_2$ is equal to one [17]. Let us group the states as $\boldsymbol{h}_{\mathrm{f}} = [h_1, \ldots, h_N]^{\top}$, $\boldsymbol{h}_l = [h_{N+1}, \ldots, h_{N+M}]^{\top}$, $\boldsymbol{x}_{\mathrm{f}} = [x_1, \ldots, x_N]^{\top}$, and $\boldsymbol{x}_l = [x_{N+1}, \ldots, x_{N+M}]^{\top}$. From [17], the dynamic convex hull spanned by the leaders can be denoted by $-\boldsymbol{\mathcal{L}}_1^{-1}\boldsymbol{\mathcal{L}}_2\boldsymbol{h}_l$ and $-\boldsymbol{\mathcal{L}}_1^{-1}\boldsymbol{\mathcal{L}}_2\boldsymbol{x}_l$. Therefore, the formation-containment errors of the vertical dynamics are defined as

$$\boldsymbol{\delta}_{\mathrm{v},i} = \boldsymbol{h}_{\mathrm{f}}^{(i-1)} + \boldsymbol{\mathcal{L}}_1^{-1}\boldsymbol{\mathcal{L}}_2\boldsymbol{h}_l^{(i-1)},\ i = 1, \ldots, 4. \tag{7}$$

Similarly and iteratively, the formation-containment errors of forward dynamics are defined as

$$\boldsymbol{\delta}_{\mathrm{f},i} = \boldsymbol{x}_{\mathrm{f}}^{(i-1)} + \boldsymbol{\mathcal{L}}_1^{-1}\boldsymbol{\mathcal{L}}_2\boldsymbol{x}_l^{(i-1)},\ i = 1, 2. \tag{8}$$

The following results will be used for subsequent stability analysis.

Lemma 1 ([27]): Define the following vectors and matrices:

$$\begin{cases} \boldsymbol{q} = [q_1, \ldots, q_N]^{\top} = \boldsymbol{\mathcal{L}}_1^{-1}\underline{\boldsymbol{1}}_N, \\ \boldsymbol{P} = \mathrm{diag}\{p_i\} = \mathrm{diag}\{1/q_i\}, \\ \boldsymbol{Q} = \boldsymbol{P}\boldsymbol{\mathcal{L}}_1 + \boldsymbol{\mathcal{L}}_1^{\top}\boldsymbol{P}. \end{cases} \tag{9}$$

Then, it holds that $\boldsymbol{P} = \boldsymbol{P}^{\top} > 0$ and $\boldsymbol{Q} = \boldsymbol{Q}^{\top} > 0$.

The goal is to design the nonrecursive event-triggered formation-containment control protocol for $\delta_{i,\mathrm{e}}^{\mathrm{c}}$ and Φ_i^{c} such that $\boldsymbol{\delta}_{\mathrm{v},i}$ and $\boldsymbol{\delta}_{\mathrm{f},i}$ converge to zero, i.e., the follower outputs $\boldsymbol{x}_{\mathrm{f}}$ and $\boldsymbol{h}_{\mathrm{f}}$ converge to the convex hull spanned by the leader HFVs, while the leader HFVs maintain a geometric space configuration.

III. Control Design for Vertical Dynamics

This section first presents the error-filtered vertical dynamics, based on which a fixed-time state observer will be devised to estimate the unknown flight states γ_i, α_i, q_i, and V_i. Then, a new event-triggered communication mechanism and formation-containment control protocol will be designed.

A. Filtered Error Dynamics

By defining a new set of states $\{\chi_{i,j}\}$, $j = 1, \ldots, 4$, a system transformation is conducted to convert the vertical dynamics (5) into the following Brunovsky form [8]:

$$\begin{aligned} \chi_{i,1} &= h_i,\ \chi_{i,2} = \dot{\chi}_{i,1} = V_i\gamma_i + d_{i,1}, \\ \chi_{i,3} &= \dot{\chi}_{i,2} = \frac{\partial\chi_{i,2}}{\partial h_i}\dot{h}_i + \frac{\partial\chi_{i,2}}{\partial\gamma_i}\dot{\gamma}_i \\ &= \vartheta_{i,2} + V_i\left(\boldsymbol{\Theta}_{i,2}^{\top}(\boldsymbol{f}_{i,2} + \boldsymbol{g}_{i,2}\alpha_i) + d_{i,2}\right), \\ \chi_{i,4} &= \dot{\chi}_{i,3} = \frac{\partial\chi_{i,3}}{\partial h_i}\dot{h}_i + \frac{\partial\chi_{i,3}}{\partial\gamma_i}\dot{\gamma}_i + \frac{\partial\chi_{i,3}}{\partial\alpha_i}\dot{\alpha}_i \\ &= \vartheta_{i,3} + V_i\boldsymbol{\Theta}_{i,2}^{\top}\boldsymbol{g}_{i,2}\left(\boldsymbol{\Theta}_{i,3}^{\top}(\boldsymbol{f}_{i,3} + \boldsymbol{g}_{i,3}q_i) + d_{i,3}\right). \end{aligned} \tag{10}$$

Denoting $\boldsymbol{\chi}_{i,j} = [\chi_{i,1}, \ldots, \chi_{i,4}]^{\top}$, we can rewrite (10) in the following compact form:

$$\dot{\boldsymbol{\chi}}_{i,4} = \boldsymbol{A}_{\mathrm{v}}\boldsymbol{\chi}_{i,4} + \boldsymbol{B}_{\mathrm{v}}\left(\vartheta_{i,4} + \mathcal{G}_{i,4}(h_i, \gamma_i, \alpha_i, q_i)\delta_i^{\mathrm{e,c}}\right) \tag{11}$$

where $\boldsymbol{A}_{\rm v}=\left[\begin{smallmatrix}\mathbf{0}_3 & \boldsymbol{I}_3\\ 0 & \mathbf{0}_3^{\top}\end{smallmatrix}\right]$, $\boldsymbol{B}_{\rm v}=\left[\begin{smallmatrix}\mathbf{0}_3\\ 1\end{smallmatrix}\right]$, $\vartheta_{i,4}=\frac{\partial\chi_{i,4}}{\partial h_i}\dot{h}_i+\frac{\partial\chi_{i,4}}{\partial\gamma_i}\dot{\gamma}_i+\frac{\partial\chi_{i,4}}{\partial\alpha_i}\dot{\alpha}_i+V_i\boldsymbol{\Theta}_{i,2}^{\top}\boldsymbol{g}_{i,2}\boldsymbol{\Theta}_{i,3}^{\top}\boldsymbol{g}_{i,3}(\boldsymbol{\Theta}_{i,4}^{\top}\boldsymbol{f}_{i,4}+d_{i,4})+\mathcal{G}_{i,4}(\delta_i^{\rm e}-\delta_i^{\rm e,c})$, and $\mathcal{G}_{i,4}=V_i\boldsymbol{\Theta}_{i,2}^{\top}\boldsymbol{g}_{i,2}\boldsymbol{\Theta}_{i,3}^{\top}\boldsymbol{g}_{i,3}\boldsymbol{\Theta}_{i,4}^{\top}\boldsymbol{g}_{i,4}$.

Denote the relative state errors of the ith follower HFV as $e_{i,1}=\sum_{k\in\mathcal{N}_i}a_{i,k}(\chi_{i,1}-\chi_{k,1}),\ldots,e_{i,4}=\sum_{k\in\mathcal{N}_i}a_{i,k}(\chi_{i,4}-\chi_{k,4})$. Define $\boldsymbol{e}_{\rm v}^1=[e_{1,1},\ldots,e_{N,1}]^{\top}=\boldsymbol{\mathcal{L}}_1\boldsymbol{h}_{\rm f}+\boldsymbol{\mathcal{L}}_2\boldsymbol{h}_l,\ldots,\boldsymbol{e}_{\rm v}^4=[e_{1,4},\ldots,e_{N,4}]^{\top}=\boldsymbol{\mathcal{L}}_1\boldsymbol{h}_{\rm f}^{(3)}+\boldsymbol{\mathcal{L}}_2\boldsymbol{h}_l^{(3)}$. Therefore, the error dynamics (11) can be rewritten as

$$\begin{cases}\dot{\boldsymbol{e}}_{\rm v}^i=\boldsymbol{e}_{\rm v}^{i+1}, & i=1,\ldots,3,\\ \dot{\boldsymbol{e}}_{\rm v}^4=\boldsymbol{\mathcal{L}}_1\left(\boldsymbol{\Gamma}_{\rm v}(\boldsymbol{v}_{\rm v})+\boldsymbol{G}_{{\rm v},4}\boldsymbol{\delta}^{\rm e,c}+\boldsymbol{\mathcal{L}}_1^{-1}\boldsymbol{\mathcal{L}}_2\boldsymbol{h}_l^{(4)}\right)\end{cases}\tag{12}$$

where $\boldsymbol{G}_{{\rm v},4}=\mathrm{diag}[\mathcal{G}_{1,4},\ldots\mathcal{G}_{N,4}]$, $\boldsymbol{\delta}^{\rm e,c}=[\delta_1^{\rm e,c},\ldots,\delta_N^{\rm e,c}]^{\top}$, $\boldsymbol{\Gamma}_{\rm v}(\boldsymbol{v}_{\rm v})=[\Gamma_{{\rm v},1}(\boldsymbol{v}_{{\rm v},1}),\ldots,\Gamma_{{\rm v},N}(\boldsymbol{v}_{{\rm v},N})]^{\top}$ with $\Gamma_{{\rm v},i}(\boldsymbol{v}_{{\rm v},i})=\vartheta_{i,4}$, $\boldsymbol{v}_{\rm v}=[\boldsymbol{v}_{{\rm v},1}^{\top},\ldots,\boldsymbol{v}_{{\rm v},N}^{\top}]^{\top}$, and $\boldsymbol{v}_{{\rm v},i}=[h_i,\gamma_i,\alpha_i,q_i]^{\top}$. Similarly to [11], we adopt a fuzzy logic system (FLS) to approximate system uncertainties $\Gamma_{{\rm v},i}(\boldsymbol{v}_{{\rm v},i})$ as $\Gamma_{{\rm v},i}(\boldsymbol{v}_{{\rm v},i})=\boldsymbol{W}_{{\rm v},i}^{\top}\boldsymbol{S}_{{\rm v},i}(\boldsymbol{v}_{{\rm v},i})+\epsilon_{{\rm v},i}$, where $\boldsymbol{W}_{{\rm v},i}$ and $\boldsymbol{S}_{{\rm v},i}(\boldsymbol{v}_{{\rm v},i})$, respectively, denote the ideal parameter vector and the fuzzy basic function vector, and $\epsilon_{{\rm v},i}$ is the approximation error satisfying $|\epsilon_{{\rm v},i}|\le\epsilon_{{\rm v},i}^*$ with $\epsilon_{{\rm v},i}^*$ being an unknown constant. For subsequent design, let us define the following sliding mode error:

$$\boldsymbol{\eta}_{\rm v}=[\eta_{{\rm v},1},\ldots,\eta_{{\rm v},N}]^{\top}=\lambda_1\boldsymbol{e}_{\rm v}^1+\lambda_2\boldsymbol{e}_{\rm v}^2+\lambda_3\boldsymbol{e}_{\rm v}^3+\boldsymbol{e}_{\rm v}^4$$

where λ_1, λ_2, and λ_3 are design parameters, which are chosen such that the polynomial $s^3+\lambda_3s^2+\lambda_2s+\lambda_1$ is Hurwitz. Let $\boldsymbol{e}_{\rm v}=[\boldsymbol{e}_{{\rm v},1}^{\top},\ldots,\boldsymbol{e}_{{\rm v},N}^{\top}]^{\top}$ and $\boldsymbol{e}_{{\rm v},i}=[e_{i,1},\ldots,e_{i,4}]^{\top}$. Then, we have

$$\boldsymbol{\eta}_{\rm v}=(\boldsymbol{I}_N\otimes\boldsymbol{\lambda}_1)\begin{bmatrix}\boldsymbol{e}_{{\rm v},1}\\ \vdots\\ \boldsymbol{e}_{{\rm v},N}\end{bmatrix}\tag{13}$$

where $\boldsymbol{\lambda}_1=[\lambda_1,\lambda_2,\lambda_3,1]$. Taking the time derivative of $\boldsymbol{\eta}_{\rm v}$ gives

$$\dot{\boldsymbol{\eta}}_{\rm v}=\boldsymbol{\psi}_{\rm v}+\boldsymbol{\mathcal{L}}_1\left(\boldsymbol{\Gamma}_{\rm v}(\boldsymbol{v}_{\rm v})+\boldsymbol{G}_{{\rm v},4}\boldsymbol{\delta}^{\rm e,c}+\boldsymbol{\mathcal{L}}_1^{-1}\boldsymbol{\mathcal{L}}_2\boldsymbol{h}_l^{(4)}\right)\tag{14}$$

where $\boldsymbol{\psi}_{\rm v}=\lambda_1\boldsymbol{e}_{\rm v}^2+\lambda_2\boldsymbol{e}_{\rm v}^3+\lambda_3\boldsymbol{e}_{\rm v}^4$. Let $\boldsymbol{E}_{\rm v}^1=[\boldsymbol{e}_{\rm v}^1,\boldsymbol{e}_{\rm v}^2,\boldsymbol{e}_{\rm v}^3]\in\mathbb{R}^{N\times3}$. The time derivative of $\boldsymbol{E}_{\rm v}^1$ can be expressed as

$$\dot{\boldsymbol{E}}_{\rm v}^1=\boldsymbol{E}_{\rm v}^1\boldsymbol{\mathcal{H}}_{\rm v}^{\top}+\boldsymbol{\eta}_{\rm v}\boldsymbol{l}_{\rm v}\tag{15}$$

where $\boldsymbol{\mathcal{H}}_{\rm v}=\begin{bmatrix}0&1&0\\0&0&1\\-\lambda_1&-\lambda_2&-\lambda_3\end{bmatrix}\in\mathbb{R}^{3\times3}$ and $\boldsymbol{l}_{\rm v}=[0,0,1]^T$. Note that $\boldsymbol{\psi}_{\rm v}=\dot{\boldsymbol{E}}_{\rm v}^1\boldsymbol{\lambda}_{\rm v}$ with $\boldsymbol{\lambda}_{\rm v}=[\lambda_1,\lambda_2,\lambda_3]^{\top}\in\mathbb{R}^3$. Because $\boldsymbol{\mathcal{H}}_{\rm v}$ is Hurwitz, given any positive constant ρ, there exists a positive definite matrix $\boldsymbol{P}_{\rm v}=\boldsymbol{P}_{\rm v}^{\top}>0$ such that

$$\boldsymbol{\mathcal{H}}_{\rm v}^{\top}\boldsymbol{P}_{\rm v}+\boldsymbol{P}_{\rm v}\boldsymbol{\mathcal{H}}_{\rm v}=-\rho\boldsymbol{I}_3.\tag{16}$$

Remark 1: The transformation (10) converts the vertical dynamics (5) into the normal dynamics (11), based on which a nonrecursive output-feedback design framework can be constructed.

B. Fixed-Time Observer Design

A fixed-time state observer is constructed to estimate the state information $\boldsymbol{\chi}_i=[\chi_{1,i},\ldots,\chi_{N,i}]^{\top}$ as follows:

$$\begin{cases}\dot{\widehat{\boldsymbol{\chi}}}_1=\widehat{\boldsymbol{\chi}}_2-\tau_1\lceil\widehat{\boldsymbol{\chi}}_1-\boldsymbol{\chi}_1\rceil^{p_1}-\iota_1\lceil\widehat{\boldsymbol{\chi}}_1-\boldsymbol{\chi}_1\rceil^{q_1},\\ \dot{\widehat{\boldsymbol{\chi}}}_2=\widehat{\boldsymbol{\chi}}_3-\tau_2\lceil\widehat{\boldsymbol{\chi}}_1-\boldsymbol{\chi}_1\rceil^{p_2}-\iota_2\lceil\widehat{\boldsymbol{\chi}}_1-\boldsymbol{\chi}_1\rceil^{q_2},\\ \dot{\widehat{\boldsymbol{\chi}}}_3=\widehat{\boldsymbol{\chi}}_4-\tau_3\lceil\widehat{\boldsymbol{\chi}}_1-\boldsymbol{\chi}_1\rceil^{p_3}-\iota_3\lceil\widehat{\boldsymbol{\chi}}_1-\boldsymbol{\chi}_1\rceil^{q_3},\\ \dot{\widehat{\boldsymbol{\chi}}}_4=-\tau_4\lceil\widehat{\boldsymbol{\chi}}_1-\boldsymbol{\chi}_1\rceil^{p_4}-\iota_4\lceil\widehat{\boldsymbol{\chi}}_1-\boldsymbol{\chi}_1\rceil^{q_4}\end{cases}\tag{17}$$

where $\widehat{\boldsymbol{\chi}}_i=[\widehat{\chi}_{1,i},\ldots,\widehat{\chi}_{N,i}]^{\top}$, $\boldsymbol{\chi}_1$ is the output vector that can be measured, and the positive design parameters $p_i>1$ and $q_i<1$, $i=1,\ldots,4$ satisfy the recurrent relations $p_i=ip_1-i+1$ and $q_i=iq_1-i+1$, $i=2,\ldots,4$, with $p_1\in(1,1+\varepsilon_p)$ and $q_1\in(1-\varepsilon_q,1)$ for sufficiently small positive constants ε_p and ε_q. Furthermore, the observer gains τ_i and ι_i, $i=1,\ldots,4$, are selected such that the matrices

$$\boldsymbol{\Gamma}_\tau=\begin{bmatrix}-\tau_1&1&0&0\\-\tau_2&0&1&0\\-\tau_3&0&0&1\\-\tau_4&0&0&0\end{bmatrix},\boldsymbol{\Gamma}_\iota=\begin{bmatrix}-\iota_1&1&0&0\\-\iota_2&0&1&0\\-\iota_3&0&0&1\\-\iota_4&0&0&0\end{bmatrix}\tag{18}$$

are Hurwitz. Then, the following lemma holds.

Lemma 2: Consider the state observer (17). The observation error vector $\widetilde{\boldsymbol{\chi}}_i=\boldsymbol{\chi}_i-\widehat{\boldsymbol{\chi}}_i$ is bounded and converges to the origin in fixed time, where an upper bound on the convergence time is given by

$$T_{\max}\triangleq\frac{\lambda_{\max}^{2-q_l}(\boldsymbol{P}_\iota)}{(1-q_l)\lambda_{\min}(\boldsymbol{Q}_\iota)}+\frac{\lambda_{\max}(\boldsymbol{P}_\tau)}{(p_1-1)\xi^{p_1-1}\lambda_{\min}(\boldsymbol{Q}_\tau)}$$

where $0<\xi\le\lambda_{\min}(\boldsymbol{P}_\tau)$, and the symmetric positive-definite matrices $\boldsymbol{P}_\tau$, $\boldsymbol{P}_\iota$, $\boldsymbol{Q}_\tau$, and $\boldsymbol{Q}_\iota$ satisfy the following relations:

$$\boldsymbol{P}_\tau\boldsymbol{\Gamma}_\tau+\boldsymbol{\Gamma}_\tau^T\boldsymbol{P}_\tau=-\boldsymbol{Q}_\tau,\quad\boldsymbol{P}_\iota\boldsymbol{\Gamma}_\iota+\boldsymbol{\Gamma}_\iota^T\boldsymbol{P}_\iota=-\boldsymbol{Q}_\iota$$

where the matrices $\boldsymbol{\Gamma}_\tau$ and $\boldsymbol{\Gamma}_\iota$ are defined in (18).

Proof: The proof of Lemma 2 is similar to [6, Theorem 2] and is, thus, omitted for space limitations. ■

C. Novel Event-Triggered Communication Mechanism

In the context of event-triggered communication, each follower HFV transmits its sliding mode error $\boldsymbol{\eta}_{\rm v}$ to its neighbors only when a prespecified event is triggered. Therefore, zero-order holder is utilized to retain the sliding mode errors sampled by the last event until the arrival of next. The latest broadcast sliding mode error of the ith HFV is denoted as $\widehat{\eta}_{{\rm v},i}(t_{k_i}^i)$, and the latest received sliding mode error from the jth HFV is denoted as $\widehat{\eta}_{{\rm v},j}(t_{k_j}^j)$, where $i,j\in F$, $j\in\mathcal{N}_i^{\dashv}$, $t_{k_i}^i$, and $t_{k_j}^j$ are event time instants with k_i, $k_j\in\mathbb{N}^+$. Note that the broadcast $\widehat{\eta}_{{\rm v},i}(t_{k_i}^i)$ remains constant in the time interval $[t_{k_i}^i,t_{k_i+1}^i)$. For the ith HFV, the sampling error is defined as $\breve{\eta}_{{\rm v},i}(t)=\widehat{\eta}_{{\rm v},i}(t_{k_i}^i)-\widehat{\eta}_{{\rm v},i}(t)$. Define a new triggering function as

$$t_{k_i+1}^i=\inf\left\{t\in\mathbb{R}^+|\,\mathcal{T}_{{\rm v},i}(t)\ge0\right\}\tag{19}$$

where

$$\mathcal{T}_{{\rm v},i}(t)=-\frac{\tau_{\rm v}||\hat{\boldsymbol{e}}_{{\rm v},i}(t)||+c_{\rm v}^1\exp(-e_{i,1}^2(t)-c_{\rm v}^0)}{l_{\rm v}\sigma_{\max}(\boldsymbol{P})\sigma_{\max}(\boldsymbol{\mathcal{L}}_1)\sigma_{\max}(\boldsymbol{\mathcal{L}}_\dashv)+\mathcal{O}_{\rm v}}+||\breve{\boldsymbol{e}}_{{\rm v},i}(t)||$$

with $\breve{\boldsymbol{e}}_{\mathrm{v},i} = \boldsymbol{e}_{\mathrm{v},i}(t^i_{k_i}) - \boldsymbol{e}_{\mathrm{v},i}(t)$, and where τ_v, l_v, $\mathcal{O}_\mathrm{v}$, c^1_v, and c^0_v are positive design parameters.

Remark 2: Existing results consider three sorts of event-triggering mechanisms, i.e., fixed threshold [20, (13)], relative threshold [20, (24)], and switching threshold [20, (28)] (cf., [21], [22], [25], and [27]). In (19), an error-dependent monotonically decreasing exponential term $c^1_\mathrm{v}\exp(-e^2_{i,1}(t) - c^0_\mathrm{v})$ has been delicately embedded into the dynamic triggering threshold, which can be considered a new typology of triggering mechanism. The simulations will show that this mechanism not only reduces the frequency of data transmission among HFVs but also guarantees the desired tracking accuracy.

D. Formation-Containment Control Protocol Design

To stabilize the sliding mode error dynamics, the formation-containment control law is constructed as

$$\begin{aligned}\boldsymbol{\delta}^{\mathrm{e,c}} = \boldsymbol{G}^{-1}_{\mathrm{v},4}\Big(&-k_\mathrm{v}\widehat{\boldsymbol{\eta}}_\mathrm{v} - \widehat{\boldsymbol{W}}^{\top}_{\mathrm{v}}\boldsymbol{S}_\mathrm{v}(\hat{\boldsymbol{v}}_\mathrm{v}) - l_\mathrm{v}\boldsymbol{\Xi}_\mathrm{v}\\ &-\boldsymbol{\mathcal{L}}^{-1}_1\boldsymbol{\mathcal{L}}_2\boldsymbol{h}^{(4)}_l - \boldsymbol{\mathcal{D}}^{-1}_1\widehat{\boldsymbol{\psi}}_\mathrm{v} - \widehat{\boldsymbol{\epsilon}}_\mathrm{v}\Big)\end{aligned} \tag{20}$$

where $\widehat{\boldsymbol{W}}_\mathrm{v} = [\widehat{\boldsymbol{W}}^{\top}_{\mathrm{v},1},\ldots,\widehat{\boldsymbol{W}}^{\top}_{\mathrm{v},N}]^{\top}$ with $\widehat{\boldsymbol{W}}_{\mathrm{v},i}$ being the estimate of $\boldsymbol{W}_{\mathrm{v},i}$, $\boldsymbol{S}_\mathrm{v}(\hat{\boldsymbol{v}}_\mathrm{v}) = [\boldsymbol{S}^{\top}_{\mathrm{v},1}(\hat{\boldsymbol{v}}_{\mathrm{v},1}),\ldots,\boldsymbol{S}^{\top}_{\mathrm{v},N}(\hat{\boldsymbol{v}}_{\mathrm{v},N})]^{\top}$, $\widehat{\boldsymbol{\epsilon}}_\mathrm{v} = [\widehat{\epsilon}_{\mathrm{v},1},\ldots,\widehat{\epsilon}_{\mathrm{v},N}]^{\top}$ with $\widehat{\epsilon}_{\mathrm{v},i}$ being the estimate of $\epsilon_{\mathrm{v},i}$, k_v and l_v are positive design parameters, and

$$\boldsymbol{\Xi}_\mathrm{v} = \begin{bmatrix}\sum_{j\in\mathcal{N}^1_\dashv} a_{1,j}\left(\widehat{\eta}_1(t^1_{k_1}) - \widehat{\eta}_j(t^j_{k_j})\right)\\ \vdots\\ \sum_{j\in\mathcal{N}^N_\dashv} a_{N,j}\left(\widehat{\eta}_N(t^N_{k_N}) - \widehat{\eta}_j(t^j_{k_j})\right)\end{bmatrix}.$$

Accordingly, the adaptation parameters are updated by

$$\begin{cases}\dot{\widehat{\boldsymbol{W}}}_\mathrm{v} = \boldsymbol{\Gamma}^w_\mathrm{v}\left(\boldsymbol{S}_\mathrm{v}(\hat{\boldsymbol{v}}_\mathrm{v})\widehat{\boldsymbol{\eta}}^{\top}_\mathrm{v}\boldsymbol{P}\boldsymbol{\mathcal{D}}_1 - \sigma^w_\mathrm{v}\widehat{\boldsymbol{W}}_\mathrm{v}\right),\\ \dot{\widehat{\boldsymbol{\epsilon}}}_\mathrm{v} = \boldsymbol{\Gamma}^\epsilon_\mathrm{v}\left(\boldsymbol{\mathcal{D}}_1\boldsymbol{P}\widehat{\boldsymbol{\eta}}_\mathrm{v} - \sigma^\epsilon_\mathrm{v}\widehat{\boldsymbol{\epsilon}}_\mathrm{v}\right)\end{cases} \tag{21}$$

where σ^w_v and $\sigma^\epsilon_\mathrm{v}$ are positive σ-modification parameters, $\boldsymbol{\Gamma}^w_\mathrm{v} = \boldsymbol{L}^w_\mathrm{v}\otimes\boldsymbol{I}_p$, $\boldsymbol{L}^w_\mathrm{v} = \mathrm{diag}[\Gamma^w_1,\ldots,\Gamma^w_N]$, $\boldsymbol{\Gamma}^\epsilon_\mathrm{v} = \mathrm{diag}[\Gamma^\epsilon_1,\ldots,\Gamma^\epsilon_N]$, with Γ^w_i and Γ^ϵ_i being positive design parameters.

Substituting (20) into (14), the dynamics of the sliding mode error can be described by

$$\begin{aligned}\dot{\boldsymbol{\eta}}_\mathrm{v} = \boldsymbol{\mathcal{L}}_1\Big(&-k_\mathrm{v}\widehat{\boldsymbol{\eta}}_\mathrm{v} + \boldsymbol{W}^{\top}_\mathrm{v}\boldsymbol{S}_\mathrm{v}(\boldsymbol{v}_\mathrm{v}) - l_\mathrm{v}\boldsymbol{\Xi}_\mathrm{v}\\ &-\widehat{\boldsymbol{W}}^{\top}_\mathrm{v}\boldsymbol{S}_\mathrm{v}(\hat{\boldsymbol{v}}_\mathrm{v}) - \boldsymbol{\mathcal{D}}^{-1}_1\widehat{\boldsymbol{\psi}}_\mathrm{v} + \widetilde{\boldsymbol{\epsilon}}_\mathrm{v}\Big) + \boldsymbol{\psi}_\mathrm{v}\end{aligned} \tag{22}$$

where $\widetilde{\boldsymbol{\epsilon}}_\mathrm{v} = \boldsymbol{\epsilon}_\mathrm{v} - \widehat{\boldsymbol{\epsilon}}_\mathrm{v}$ with $\boldsymbol{\epsilon}_\mathrm{v} = [\epsilon_{\mathrm{v},1},\ldots,\epsilon_{\mathrm{v},N}]^{\top}$.

Remark 3: The proposed control law (20) comprises a linear term $-k_\mathrm{v}\widehat{\boldsymbol{\eta}}_\mathrm{v}$ and a nonlinear event-trigger term $-l_\mathrm{v}\boldsymbol{\Xi}_\mathrm{v}$. The linear feedback protocol $-k_\mathrm{v}\widehat{\boldsymbol{\eta}}_\mathrm{v}$ contains all the information from the neighbors of the ith follower HFV, which is utilized to guide the follower HFVs toward the convex hull formed by the leader HFVs. The nonlinear event-trigger term $-l_\mathrm{v}\boldsymbol{\Xi}_\mathrm{v}$ is designed in such a way that the discrepancy between current and desired configuration is reduced timely and that formations can be achieved during the maneuvering process.

IV. Stability Analysis for Vertical Dynamics

Stability analysis and exclusion of Zeno behavior of the proposed event-triggered control protocol will be presented in this section.

A. Main Result

Theorem 1: Consider the closed-loop system composed of the vertical dynamics (10) of HFV swarm system, by the event-triggered communication mechanism (19), by the formation-containment control protocol (20), and the adaptation laws (21). Let the control gain k_v satisfy

$$k_\mathrm{v} > \frac{2}{\sigma_{\min}(\boldsymbol{Q})}\left(\frac{2\xi^2}{\rho} + \frac{\vartheta^2}{\sigma^w_\mathrm{v}} + \frac{\varsigma^2}{\sigma^\epsilon_\mathrm{v}} + \varphi\right) \tag{23}$$

where

$$\begin{aligned}&\varsigma = -\frac{\sigma_{\max}(\boldsymbol{P})\sigma_{\max}(\boldsymbol{\mathcal{A}}_1)}{2},\ \vartheta = -\frac{\sigma_{\max}(\boldsymbol{P})\sigma_{\max}(\boldsymbol{\mathcal{A}}_1)\bar{S}_\mathrm{v}}{2},\\ &\xi = -\frac{\sigma_{\max}(\boldsymbol{P})\sigma_{\max}(\boldsymbol{\mathcal{A}}_1)}{2\sigma_{\min}(\boldsymbol{\mathcal{D}}_1)}\,||\boldsymbol{\mathcal{H}}_\mathrm{v}||\,||\boldsymbol{\lambda}_\mathrm{v}|| - \frac{\sigma_{\max}(\boldsymbol{P}_\mathrm{v})}{2},\\ &\phi = \frac{k_\mathrm{v}\sigma_{\min}(\boldsymbol{Q})}{2} - \varphi,\ \varphi = \frac{\sigma_{\max}(\boldsymbol{P})\sigma_{\max}(\boldsymbol{\mathcal{A}}_1)}{\sigma_{\min}(\boldsymbol{\mathcal{D}}_1)}||\boldsymbol{\lambda}_\mathrm{v}||\\ &\quad + l_\mathrm{v}\sigma_{\max}(\boldsymbol{P})\sigma_{\max}(\boldsymbol{\mathcal{L}}_1)\sigma_{\max}(\boldsymbol{\mathcal{L}}_\dashv) + \tau_\mathrm{v}.\end{aligned}$$

Then, all signals in the resulting closed-loop system remain semiglobally uniformly ultimately bounded, and the formation-containment errors $\boldsymbol{\delta}_{\mathrm{v},i}$ between the leader HFVs and the follower HFVs converge to an adjustable neighborhood of the origin.

Proof: Consider the Lyapunov function candidate

$$\begin{aligned}\mathfrak{L}_\mathrm{v} = &\frac{1}{2}\boldsymbol{\eta}^{\top}_\mathrm{v}\boldsymbol{P}\boldsymbol{\eta}_\mathrm{v} + \frac{1}{2}\mathrm{tr}\left(\boldsymbol{E}^1_\mathrm{v}\boldsymbol{P}_\mathrm{v}\boldsymbol{E}^{1\,\top}_\mathrm{v}\right)\\ &+ \frac{1}{2}\mathrm{tr}\left(\widetilde{\boldsymbol{W}}^{\top}_\mathrm{v}\boldsymbol{\Gamma}^{w-1}_\mathrm{v}\widetilde{\boldsymbol{W}}_\mathrm{v}\right) + \frac{1}{2}\widetilde{\boldsymbol{\epsilon}}^{\top}_\mathrm{v}\boldsymbol{\Gamma}^{\epsilon-1}_\mathrm{v}\widetilde{\boldsymbol{\epsilon}}_\mathrm{v}\end{aligned} \tag{24}$$

where $\widetilde{\boldsymbol{W}}_\mathrm{v} = [\widetilde{\boldsymbol{W}}^{\top}_{\mathrm{v},1},\ldots,\widetilde{\boldsymbol{W}}^{\top}_{\mathrm{v},N}]^{\top}$, $\widetilde{\boldsymbol{W}}^{\top}_{\mathrm{v},i} = \boldsymbol{W}^{\top}_{\mathrm{v},i} - \widehat{\boldsymbol{W}}^{\top}_{\mathrm{v},i}$.

Differentiating $\mathfrak{L}_\mathrm{v}$ along (23) and (24) yields

$$\begin{aligned}\dot{\mathfrak{L}}_\mathrm{v} = &-\frac{k_\mathrm{v}}{2}\boldsymbol{\eta}^{\top}_\mathrm{v}\boldsymbol{Q}\boldsymbol{\eta}_\mathrm{v} - \frac{\rho}{2}\mathrm{tr}\left(\boldsymbol{E}^1_\mathrm{v}\boldsymbol{E}^{1\,\top}_\mathrm{v}\right) + \boldsymbol{\eta}^{\top}_\mathrm{v}\boldsymbol{P}\boldsymbol{\mathcal{A}}_1\boldsymbol{\mathcal{D}}^{-1}_1\boldsymbol{\psi}_\mathrm{v}\\ &- l_\mathrm{v}\boldsymbol{\eta}^{\top}_\mathrm{v}\boldsymbol{P}\boldsymbol{\mathcal{L}}_1\boldsymbol{\mathcal{L}}_\dashv\widehat{\boldsymbol{\eta}}_\mathrm{v} - l_\mathrm{v}\boldsymbol{\eta}^{\top}_\mathrm{v}\boldsymbol{P}\boldsymbol{\mathcal{L}}_1\boldsymbol{\mathcal{L}}_\dashv\breve{\boldsymbol{\eta}}_\mathrm{v} + \sigma^\epsilon_\mathrm{v}\widetilde{\boldsymbol{\epsilon}}^{\top}_\mathrm{v}\widehat{\boldsymbol{\epsilon}}_\mathrm{v}\\ &+ \boldsymbol{\eta}^{\top}_\mathrm{v}\boldsymbol{P}\boldsymbol{\mathcal{L}}_1\boldsymbol{W}^{\top}_\mathrm{v}\left(\boldsymbol{S}_\mathrm{v}(\boldsymbol{v}_\mathrm{v}) - \boldsymbol{S}_\mathrm{v}(\hat{\boldsymbol{v}}_\mathrm{v})\right) - \widehat{\boldsymbol{\eta}}^{\top}_\mathrm{v}\boldsymbol{P}\boldsymbol{\mathcal{A}}_1\widetilde{\boldsymbol{\epsilon}}_\mathrm{v}\\ &+ \boldsymbol{\eta}^{\top}_\mathrm{v}\boldsymbol{P}\boldsymbol{\mathcal{L}}_1\left(k_\mathrm{v}\widetilde{\boldsymbol{\eta}}_\mathrm{v} + \boldsymbol{\mathcal{D}}^{-1}_1\widetilde{\boldsymbol{\psi}}_\mathrm{v}\right) + \sigma^w_\mathrm{v}\mathrm{tr}\left(\widetilde{\boldsymbol{W}}^{\top}_\mathrm{v}\widehat{\boldsymbol{W}}_\mathrm{v}\right)\\ &+ \mathrm{tr}\left(\boldsymbol{\eta}_\mathrm{v}l_\mathrm{v}\boldsymbol{P}_\mathrm{v}\boldsymbol{E}^{\top}_{\mathrm{v},1}\right) - \widehat{\boldsymbol{\eta}}^{\top}_\mathrm{v}\boldsymbol{P}\boldsymbol{\mathcal{A}}_1\widetilde{\boldsymbol{W}}^{\top}_\mathrm{v}\boldsymbol{S}_\mathrm{v}(\hat{\boldsymbol{v}}_\mathrm{v})\\ &+ \widetilde{\boldsymbol{\eta}}^{\top}_\mathrm{v}\boldsymbol{P}\boldsymbol{\mathcal{L}}_1\widetilde{\boldsymbol{W}}^{\top}_\mathrm{v}\boldsymbol{S}_\mathrm{v}(\hat{\boldsymbol{v}}_\mathrm{v}) + \widetilde{\boldsymbol{\eta}}^{\top}_\mathrm{v}\boldsymbol{P}\boldsymbol{\mathcal{L}}_1\widetilde{\boldsymbol{\epsilon}}_\mathrm{v}\end{aligned} \tag{25}$$

where $\breve{\boldsymbol{\eta}}_\mathrm{v} = \boldsymbol{\eta}_\mathrm{v}(t^i_{k_i}) - \boldsymbol{\eta}_\mathrm{v}(t)$ is the event-triggered error vector.

According to the definition of FLS [11], there exist constants $\bar{S}_\mathrm{v} > 0$, $\bar{\epsilon}_\mathrm{v} > 0$, and $\bar{W}_\mathrm{v} > 0$ such that $||\boldsymbol{S}_\mathrm{v}|| \le \bar{S}_\mathrm{v}$, $||\boldsymbol{\epsilon}_\mathrm{v}|| \le \bar{\epsilon}_\mathrm{v}$, and $||\boldsymbol{W}_\mathrm{v}|| \le \bar{W}_\mathrm{v}$. It can be derived from $||\widetilde{\boldsymbol{\chi}}_i|| \le X_i$ (which is a result of Lemma 2) that $||\widetilde{\boldsymbol{\eta}}_\mathrm{v}|| \le \bar{\eta} \triangleq \lambda_{\max}(\boldsymbol{\mathcal{L}}_1)(\lambda_1X_1 + \lambda_2X_2 + \lambda_3X_3 + X_4)$ and

$||\widetilde{\psi}_{\rm v}|| \le \bar{\psi} \triangleq \lambda_{\max}(\mathcal{L}_1)(\lambda_1 X_2 + \lambda_2 X_3 + \lambda_3 X_4)$. Then, it follows from (19) that $l_{\rm v}\sigma_{\max}(\boldsymbol{P})\sigma_{\max}(\mathcal{L}_1)\sigma_{\max}(\mathcal{L}_\dashv)||\check{e}_{{\rm v},i}(t)|| < \tau_{\rm v}||\hat{e}_{{\rm v},i}(t)|| + c_{\rm v}^1\exp(-c_{\rm v}^0)$ holds on $[0,t)$, which allows us to rewrite (25) as

$$\begin{aligned}\dot{\mathfrak{L}}_{\rm v} \le & -\frac{k_{\rm v}}{2}\sigma_{\min}(\boldsymbol{Q})\boldsymbol{\eta}_{\rm v}^\top\boldsymbol{\eta}_{\rm v} - \frac{\rho}{2}{\rm tr}\left(\boldsymbol{E}_{\rm v}^1\boldsymbol{E}_{\rm v}^{1\top}\right) - \sigma_{\rm v}^w{\rm tr}\left(\widetilde{\boldsymbol{W}}_{\rm v}^\top\widetilde{\boldsymbol{W}}_{\rm v}\right)\\ & - \sigma_{\rm v}^\epsilon\widetilde{\boldsymbol{\epsilon}}_{\rm v}^\top\widetilde{\boldsymbol{\epsilon}}_{\rm v} + \|\boldsymbol{\eta}_{\rm v}\|^2(l_{\rm v}\sigma_{\max}(\boldsymbol{P})\sigma_{\max}(\mathcal{L}_1)\sigma_{\max}(\mathcal{L}_\dashv) + \tau_{\rm v})\\ & + \|\boldsymbol{\eta}_{\rm v}\|\sigma_{\max}(\boldsymbol{P})\sigma_{\max}(\mathcal{L}_1)(\sigma_{\min}^{-1}(\mathcal{D}_1)\bar{\psi} + 2\bar{W}_{\rm v}\bar{S}_{\rm v} + k_{\rm v}\bar{\eta})\\ & + (\|\widetilde{\boldsymbol{W}}_{\rm v}\|\bar{S}_{\rm v}\bar{\eta} + \|\widetilde{\boldsymbol{\epsilon}}_{\rm v}\|\bar{\eta})\sigma_{\max}(\boldsymbol{P})(\sigma_{\max}(\mathcal{A}_1) + \sigma_{\max}(\mathcal{L}_1))\\ & + \|\boldsymbol{\eta}_{\rm v}\|l_{\rm v}\sigma_{\max}(\boldsymbol{P})\sigma_{\max}(\mathcal{L}_1)\sigma_{\max}(\mathcal{L}_\dashv)\bar{\eta} + \|\widetilde{\boldsymbol{W}}_{\rm v}\|\sigma_{\rm v}^w\bar{W}_{\rm v}\\ & + \|\boldsymbol{\eta}_{\rm v}\|\,\|\boldsymbol{E}_{\rm v}^1\|\sigma_{\max}(\boldsymbol{P}_{\rm v}) + \|\widetilde{\boldsymbol{\epsilon}}_{\rm v}\|\sigma_{\rm v}^\epsilon\bar{\epsilon}_{\rm v} + \|\boldsymbol{\eta}_{\rm v}\|(\bar{\eta}\tau_{\rm v} + \bar{c})\\ & + (\|\boldsymbol{\eta}_{\rm v}\|\,\|\boldsymbol{E}_{\rm v}^1\|\,\|\mathcal{H}_{\rm v}\| + \|\boldsymbol{\eta}_{\rm v}\|^2)\|\boldsymbol{\lambda}_{\rm v}\|\frac{\sigma_{\max}(\boldsymbol{P})\sigma_{\max}(\mathcal{A}_1)}{\sigma_{\min}(\mathcal{D}_1)}\\ & + \|\boldsymbol{\eta}_{\rm v}\|\sigma_{\max}(\boldsymbol{P})\sigma_{\max}(\mathcal{A}_1)(\|\widetilde{\boldsymbol{W}}_{\rm v}\|\bar{S}_{\rm v} + \|\widetilde{\boldsymbol{\epsilon}}_{\rm v}\|) \end{aligned} \tag{26}$$

where $\bar{c} = ||\boldsymbol{\lambda}_1||\sqrt{N}c_{\rm v}^1\exp(-c_{\rm v}^0)$. Define $\boldsymbol{X}_{\rm v} = [\,||\boldsymbol{\eta}_{\rm v}||, ||\boldsymbol{E}_{\rm v}^1||, ||\widetilde{\boldsymbol{W}}_{\rm v}||, ||\widetilde{\boldsymbol{\epsilon}}_{\rm v}||\,]^\top$. We can rewrite the derivative of $\mathfrak{L}_{\rm v}$ as

$$\dot{\mathfrak{L}}_{\rm v} \le -\boldsymbol{X}_{\rm v}^\top\boldsymbol{\Lambda}_{\rm v}\boldsymbol{X}_{\rm v} + \boldsymbol{\Upsilon}_{\rm v}^\top\boldsymbol{X}_{\rm v} \tag{27}$$

where $\boldsymbol{\Lambda}_{\rm v} = \begin{bmatrix}\phi & \xi & \vartheta & \varsigma\\ \xi & \rho/2 & 0 & 0\\ \vartheta & 0 & \sigma_{\rm v}^w & 0\\ \varsigma & 0 & 0 & \sigma_{\rm v}^\epsilon\end{bmatrix}$, $\boldsymbol{\Upsilon}_{\rm v} = \begin{bmatrix}\mu\\ 0\\ \zeta^\star\\ \hbar\end{bmatrix}$, $\mu = \sigma_{\max}(\boldsymbol{P})\sigma_{\max}(\mathcal{L}_1)(\sigma_{\min}^{-1}(\mathcal{D}_1)\bar{\psi} + 2\bar{W}_{\rm v}\bar{S}_{\rm v} + k_{\rm v}\bar{\eta}) + l_{\rm v}\sigma_{\max}(\boldsymbol{P})\sigma_{\max}(\mathcal{L}_1)\sigma_{\max}(\mathcal{L}_\dashv)\bar{\eta} + \bar{\eta}\tau_{\rm v} + \bar{c}$, $\zeta^\star = \sigma_{\rm v}^w\bar{W}_{\rm v} + \sigma_{\max}(\boldsymbol{P})(\sigma_{\max}(\mathcal{A}_1) + \sigma_{\max}(\mathcal{L}_1))\bar{S}_{\rm v}\bar{\eta}$, and $\hbar = \sigma_{\rm v}^\epsilon\bar{\epsilon}_{\rm v} + \bar{\eta}\sigma_{\max}(\boldsymbol{P})(\sigma_{\max}(\mathcal{A}_1) + \sigma_{\max}(\mathcal{L}_1))$.

Note that the matrix $\boldsymbol{\Lambda}_{\rm v}$ is positive definite under condition (27). Therefore, inequality (27) can be further expressed as

$$\dot{\mathfrak{L}}_{\rm v} \le -\sigma_{\min}(\boldsymbol{\Lambda}_{\rm v})||\boldsymbol{X}_{\rm v}||^2 + ||\boldsymbol{\Upsilon}_{\rm v}||\,||\boldsymbol{X}_{\rm v}||. \tag{28}$$

To continue, define $\lambda_{\min} = \min\{\sigma_{\min}(\boldsymbol{\Gamma}_{\rm v}^{w-1}), \sigma_{\min}(\boldsymbol{\Gamma}_{\rm v}^{\epsilon-1}), \sigma_{\min}(\boldsymbol{P}), \sigma_{\min}(\boldsymbol{P}_{\rm v})\}$, $\lambda_{\max} = \max\{\sigma_{\max}(\boldsymbol{P}), \sigma_{\max}(\boldsymbol{P}_{\rm v}), \sigma_{\max}(\boldsymbol{\Gamma}_{\rm v}^{w-1}), \sigma_{\max}(\boldsymbol{\Gamma}_{\rm v}^{\epsilon-1})\}$. Recalling the construction of $\mathfrak{L}_{\rm v}$ in (24), one obtains $\frac{1}{2}\lambda_{\min}||\boldsymbol{X}_{\rm v}||^2 \le \mathfrak{L}_{\rm v} \le \frac{1}{2}\lambda_{\max}||\boldsymbol{X}_{\rm v}||^2$. Then, we further obtain the inequality $\dot{\mathfrak{L}}_{\rm v} \le -\beta_{\rm v}\mathfrak{L}_{\rm v} + \varpi_{\rm v}\sqrt{\mathfrak{L}_{\rm v}}$. Letting $K = \sqrt{\mathfrak{L}_{\rm v}}$, it holds that

$$2K\dot{K} \le -\beta_{\rm v}K^2 + \varpi_{\rm v}K. \tag{29}$$

Multiplying $\frac{1}{2^-K}\exp(\frac{\beta_v}{2}t)$ on both sides of inequality (29) yields

$$\left(K\exp\left(\frac{\beta_{\rm v}}{2}t\right)\right)' \le \frac{\varpi_{\rm v}}{\beta_{\rm v}}\left(\exp\left(\frac{\beta_{\rm v}}{2}t\right)\right)' \tag{30}$$

whose integral over $[0,t)$ is

$$K(t) \le K(0)\exp\left(-\frac{\beta_{\rm v}}{2}t\right) - \frac{\varpi_{\rm v}}{\beta_{\rm v}}\exp\left(-\frac{\beta_{\rm v}}{2}t\right) + \frac{\varpi_{\rm v}}{\beta_{\rm v}}. \tag{31}$$

Substituting $K = \sqrt{\mathfrak{L}_{\rm v}}$ into (31), one can finally get

$$\sqrt{\mathfrak{L}_{\rm v}(t)} \le \sqrt{\mathfrak{L}_{\rm v}(0)}\exp\left(-\frac{\beta_{\rm v}t}{2}\right) + \frac{\varpi_{\rm v}}{\beta_{\rm v}}\left[1 - \exp\left(-\frac{\beta_{\rm v}t}{2}\right)\right] \tag{32}$$

where $\beta_{\rm v} = 2\sigma_{\min}(\boldsymbol{\Lambda}_{\rm v})\lambda_{\max}^{-1}$ and $\varpi_{\rm v} = \sqrt{2\lambda_{\min}^{-1}}||\boldsymbol{\Upsilon}_{\rm v}||$. From (24) and (32), one can conclude that the error signals $\boldsymbol{\eta}_{\rm v}$, $\boldsymbol{E}_{\rm v}^1$, $\widetilde{\boldsymbol{W}}_{\rm v}$, and $\widetilde{\boldsymbol{\epsilon}}_{\rm v}$ are bounded, which further implies that the sliding mode error $\boldsymbol{\eta}_{\rm v}$ will stay near the sliding surface, i.e., the relative state error vectors $\boldsymbol{e}_{\rm v}^1, \ldots, \boldsymbol{e}_{\rm v}^4$ are bounded. Since $\boldsymbol{e}_{\rm v}^i = \mathcal{L}_1\boldsymbol{\delta}_{{\rm v},i}$, $i = 1, \ldots, 4$, the formation-containment errors are eventually upper bounded by

$$||\boldsymbol{\delta}_{{\rm v},i}|| \le \frac{||\boldsymbol{e}_{\rm v}^i||}{\sigma_{\min}(\mathcal{L}_1)}, \quad i \in \{1,2,3,4\} \tag{33}$$

which implies that all follower HFVs ultimately move into the convex hull spanned by the leader HFVs with bounded formation-containment errors. ■

B. Exclusion of Zeno Behavior

By (20), the dynamics of the relative state error in (12) can be described by $\dot{\boldsymbol{e}}_{\rm v}^1 = \boldsymbol{e}_{\rm v}^2, \ldots, \dot{\boldsymbol{e}}_{\rm v}^4 = \mathcal{L}_1\boldsymbol{\mathcal{F}}_{\rm v}$, where $\boldsymbol{\mathcal{F}}_{\rm v} = [\mathcal{F}_{{\rm v},1}, \ldots, \mathcal{F}_{{\rm v},N}]^\top = -k_{\rm v}\widehat{\boldsymbol{\eta}}_{\rm v} - l_{\rm v}\boldsymbol{\Xi}_{\rm v} - \mathcal{D}_1^{-1}\widehat{\boldsymbol{\psi}}_{\rm v} + \boldsymbol{W}_{\rm v}^\top\boldsymbol{S}_{\rm v}(\boldsymbol{v}_{\rm v}) - \widehat{\boldsymbol{W}}_{\rm v}^\top\boldsymbol{S}_{\rm v}(\hat{\boldsymbol{v}}_{\rm v}) + \widetilde{\boldsymbol{\epsilon}}_{\rm v}$. Thus, it can be derived that the inequality $||\dot{\boldsymbol{e}}_{{\rm v},i}|| \le ||\boldsymbol{\Psi}_{\rm v}||\,||\boldsymbol{e}_{{\rm v},i}|| + \mathcal{F}_{\max}$ holds, where $\mathcal{F}_{\max} = \sigma_{\max}(\mathcal{L}_1)\max_{[t_{k_i}^i, t_{k_i+1}^i)}|\mathcal{F}_{{\rm v},i}|$ and $\boldsymbol{\Psi}_{\rm v} = \begin{bmatrix}\boldsymbol{0}_3 & \boldsymbol{I}_3\\ 0 & \boldsymbol{0}_3\end{bmatrix}$. From the definition of $\check{\boldsymbol{e}}_{{\rm v},i}$ under (19), we get

$$\frac{\rm d}{{\rm d}t}||\check{\boldsymbol{e}}_{{\rm v},i}|| = \frac{\rm d}{{\rm d}t}\sqrt{\check{\boldsymbol{e}}_{{\rm v},i}^\top\check{\boldsymbol{e}}_{{\rm v},i}} = \frac{\check{\boldsymbol{e}}_{{\rm v},i}^\top\dot{\check{\boldsymbol{e}}}_{{\rm v},i}}{||\check{\boldsymbol{e}}_{{\rm v},i}||} \le ||\dot{\boldsymbol{e}}_{{\rm v},i}||. \tag{34}$$

It follows from (34) that $\frac{\rm d}{{\rm d}t}||\check{\boldsymbol{e}}_{{\rm v},i}|| \le ||\boldsymbol{\Psi}_{\rm v}||\,||\boldsymbol{e}_{{\rm v},i}|| + \mathcal{F}_{\max}$. By the comparison lemma [26], the solution of (34) with the initial condition $\boldsymbol{e}_{{\rm v},i}^+(t_{k_i}^i) = 0$ is

$$\begin{aligned}||\check{\boldsymbol{e}}_{{\rm v},i}|| &\le \mathcal{F}_{\max}\int_{t_{k_i}^{i+}}^{t}\exp(||\boldsymbol{\Psi}_{\rm v}||(t-s)){\rm d}s, \quad \forall t \in \left[t_{k_i}^i, t_{k_i+1}^i\right),\\ &\le \frac{\mathcal{F}_{\max}}{||\boldsymbol{\Psi}_{\rm v}||}\left[\exp(||\boldsymbol{\Psi}_{\rm v}||(t - t_{k_i}^i)) - 1\right]. \end{aligned} \tag{35}$$

Over all time interval, the minimum threshold value of $||\check{\boldsymbol{e}}_{{\rm v},i}||$ is defined as $\delta_{\min}$. Thence, (35) can be expressed as

$$\delta_{\min} \le \frac{\mathcal{F}_{\max}}{||\boldsymbol{\Psi}_{\rm v}||}\left[\exp(||\boldsymbol{\Psi}_{\rm v}||(t_{k_i+1}^i - t_{k_i}^i)) - 1\right]. \tag{36}$$

From (36), it is possible to arrive at

$$t_{k_i+1}^i - t_{k_i}^i \ge \frac{\ln\left(1 + \delta_{\min}||\boldsymbol{\Psi}_{\rm v}||/\mathcal{F}_{\max}\right)}{||\boldsymbol{\Psi}_{\rm v}||} > 0 \tag{37}$$

which implies that the interevent time is bounded away from zero, i.e., Zeno behavior is precluded.

TABLE I
DESIGN OF FORWARD DYNAMICS

Formation-Containment Control Law

$$\Phi^{\mathrm{c}} = \boldsymbol{G}_{\mathrm{f},2}^{-1}\Big(- k_{\mathrm{f}}\widehat{\boldsymbol{\eta}}_{\mathrm{f}} - \widehat{\boldsymbol{W}}_{\mathrm{f}}^{\top}\boldsymbol{S}_{\mathrm{f}}(\hat{\boldsymbol{v}}_{\mathrm{f}}) - l_{\mathrm{f}}\boldsymbol{\Xi}_{\mathrm{f}} - \boldsymbol{\mathcal{L}}_1^{-1}\boldsymbol{\mathcal{L}}_2\ddot{\boldsymbol{x}}_l - \boldsymbol{\mathcal{D}}_1^{-1}\dot{\widehat{\boldsymbol{\psi}}}_{\mathrm{f}} - \widehat{\boldsymbol{\epsilon}}_{\mathrm{f}}\Big),$$

Parameter Adaptation Laws

$$\dot{\widehat{\boldsymbol{W}}}_{\mathrm{f}} = \boldsymbol{\Gamma}_{\mathrm{f}}^{w}\Big(\boldsymbol{S}_{\mathrm{f}}(\hat{\boldsymbol{v}}_{\mathrm{f}})\widehat{\boldsymbol{\eta}}_{\mathrm{f}}^{\top}\boldsymbol{P}\boldsymbol{\mathcal{D}}_1 - \sigma_{\mathrm{f}}^{w}\widehat{\boldsymbol{W}}_{\mathrm{f}}\Big),$$
$$\dot{\widehat{\boldsymbol{\epsilon}}}_{\mathrm{f}} = \boldsymbol{\Gamma}_{\mathrm{f}}^{\epsilon}(\boldsymbol{\mathcal{D}}_1\boldsymbol{P}\widehat{\boldsymbol{\eta}}_{\mathrm{f}} - \sigma_{\mathrm{f}}^{\epsilon}\widehat{\boldsymbol{\epsilon}}_{\mathrm{f}}),$$

Event-Triggered Mechanism

$$t_{k_i+1}^{\mathrm{f},i} = \inf\{t \in \mathbb{R}^{+} | \mathcal{T}_{\mathrm{f},i}(t, \check{\boldsymbol{e}}_{\mathrm{f},i}(t)) \geq 0\},$$

where $\mathcal{T}_{\mathrm{f},i}(\cdot,\cdot) = ||\check{\boldsymbol{e}}_{\mathrm{f},i}(t)|| - \frac{\tau_{\mathrm{f}}||\hat{\boldsymbol{e}}_{\mathrm{f},i}(t)|| + c_{\mathrm{f}}^{1}\exp(-e_{i,1}^{\mathrm{c}}(t)^2 - c_{\mathrm{f}}^{0})}{l_{\mathrm{f}}\sigma_{\max}(\boldsymbol{P})\sigma_{\max}(\boldsymbol{\mathcal{L}}_1)\sigma_{\max}(\boldsymbol{\mathcal{L}}_{-1}) + \mathcal{O}_{\mathrm{f}}}$.

V. FORWARD CONTROL LOOP

Along similar lines to the vertical control loop, the detailed control design for forward dynamics is summarized in Table I, with error dynamics $\boldsymbol{\eta}_{\mathrm{f}} = \lambda_{\mathrm{f}}\boldsymbol{e}_{\mathrm{f}}^{1} + \boldsymbol{e}_{\mathrm{f}}^{2}$, with $\boldsymbol{e}_{\mathrm{f}}^{j} = [e_{1,j}^{\mathrm{c}}, \ldots, e_{N,j}^{\mathrm{c}}]^{\top}$, $e_{i,j}^{\mathrm{c}} = \sum_{k\in\mathcal{N}_i} a_{i,k}(\chi_{i,j}^{\mathrm{c}} - \chi_{k,j}^{\mathrm{c}})$, and system transformation $\chi_{i,j}^{\mathrm{c}} = x_i^{(j-1)}$, $j = 1, 2$. Furthermore, k_{f}, l_{f}, τ_{f}, l_{f}, $\mathcal{O}_{\mathrm{f}}$, c_{f}^{1}, and c_{f}^{0} are positive design parameters, $\boldsymbol{\Gamma}_{\mathrm{f}}^{w} = \boldsymbol{\Gamma}_{\mathrm{f}}^{w\top} > 0$, $\boldsymbol{\Gamma}_{\mathrm{f}}^{\epsilon} = \boldsymbol{\Gamma}_{\mathrm{f}}^{\epsilon\top} > 0$, σ_{f}^{w}, and $\sigma_{\mathrm{f}}^{\epsilon}$ are the σ-modification parameters, and $\boldsymbol{\Xi}_{\mathrm{f}} = [\sum_{j\in\mathcal{N}_i^{-1}} a_{i,j}(\eta_{\mathrm{f},i}(t_{k_i}^{\mathrm{f},i}) - \eta_{\mathrm{f},j}(t_{k_j}^{\mathrm{f},j}))]^{N\times 1}$. Then, the main results are given in the following theorem.

Theorem 2: Consider the closed-loop system composed of the forward dynamics of the HFV swarm system, the formation-containment control law, the parameter adaptation laws, and the event-triggered communication mechanism summarized in Table I where control gain k_{f} satisfies a condition similar to (23). Then, all closed-loop signals are semiglobally uniformly ultimately bounded and the formation-containment errors between leader HFVs and follower HFVs converge to an adjustable neighborhood of the origin.

Proof: The proof is analogous to that of Theorem 1 and is, therefore, omitted to avoid repetitions. ■

VI. SIMULATION RESULTS

To validate the effectiveness of the proposed control scheme, we consider an HFV swarm system including four leader HFVs (HFV#4-7) and three follower HFVs (HFV#1-3). The communication topology is shown in Fig. 2.

Based on practical engineering characteristics, the limitations of the actuators of the ith follower HFV are set as $\Phi_i \in [0.05, 1.2]$, $\dot{\Phi}_i \in [-1, 1]$, $\delta_i^{\mathrm{e}} \in [-20\,\mathrm{deg}, 20\,\mathrm{deg}]$, and $\dot{\delta}_i^{\mathrm{e}} \in [-20\,\mathrm{deg/s}, 20\,\mathrm{deg/s}]$. Parameters for actuator dynamics are set as $\omega = 5$ rad/s and $\zeta = 0.95$. The initial values of the vertical and forward positions of leader HFVs are $h_4(0) = 86\,000$ ft, $x_4(0) = 300$ ft, $h_5(0) = 85\,900$ ft, $x_5(0) = 700$ ft, $h_6(0) = 85\,800$ ft, $x_6(0) = 0$ ft, $h_7(0) = 85\,300$ ft, and $x_7(0) = 400$ ft. The initial values of the rigid states are $V_i(0) = 7700$ ft/s, $\gamma_i(0) = 0$ deg, $\alpha_i(0) = 1.6325$ deg, and $q_i(0) = 0$ deg/s. Besides, the initial values of the first two flexible states and their time derivatives are $\eta_{i,1}(0) = 0.9700$, $\eta_{i,2}(0) = 0.7967$, and $\dot{\eta}_{i,1}(0) = \dot{\eta}_{i,2}(0) = 0$, $i \in \{1, 2, 3\}$. The uncertain aerodynamic coefficients in (3) are modeled as $C_i = C_i^{*}(1 + \Delta_i)$, where C_i^{*} represents the nominal coefficient and Δ_i represents the uncertain factor ranging from -35% to 35%. The design parameters are chosen as: $k_{\mathrm{v}} = 25$, $k_{\mathrm{f}} = 15$, $l_{\mathrm{v}} = 5.5$,

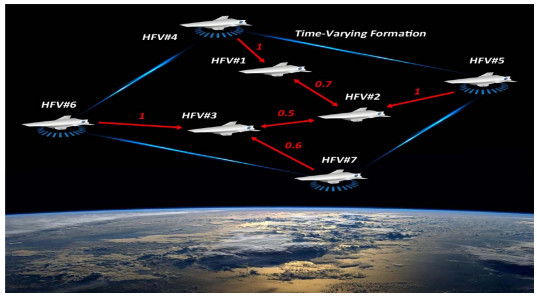

Fig. 2. Communication topology among HFVs.

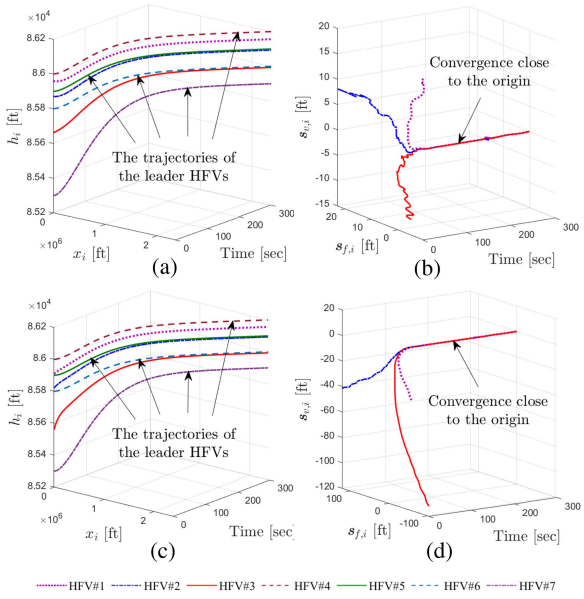

Fig. 3. Trajectories of follower HFVs and leader HFVs in (a) Case 1 and (c) Case 2. Trajectories of tracking errors of follower HFVs in (b) Case 1 and (d) Case 2.

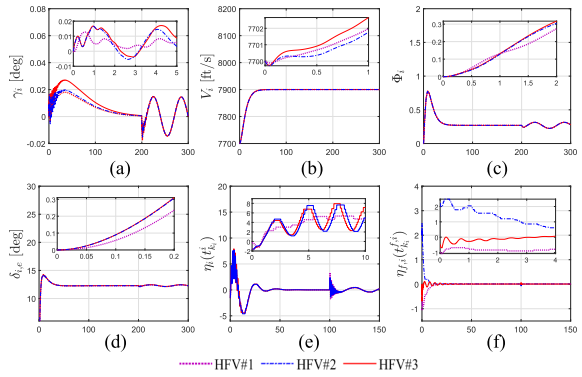

Fig. 4. Trajectories of rigid-body states, control inputs, and sliding mode errors.

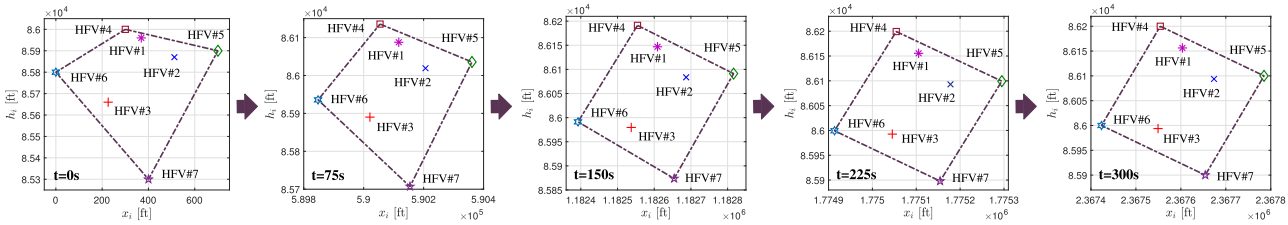

Fig. 5. Trajectories of position snapshots of follower HFVs and leader HFVs at five different time instants.

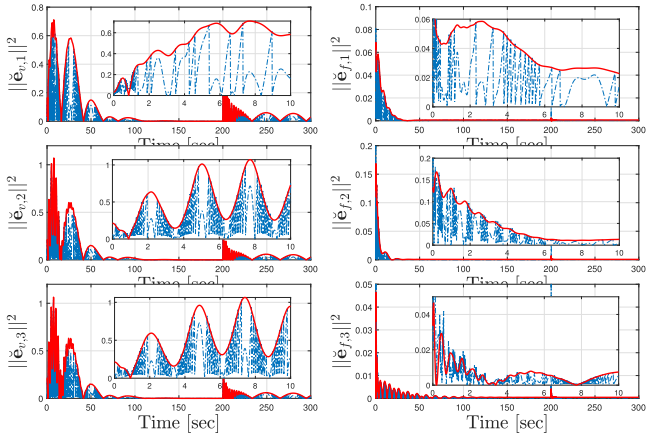

Fig. 6. Sampling errors and triggering thresholds.

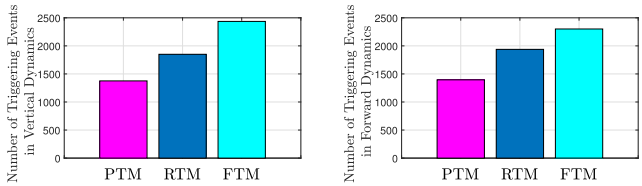

Fig. 7. Triggering times of the examined methods.

TABLE II
NUMBER OF TRIGGERING EVENTS FOR PTM, RTM, AND FTM

	Vertical Dynamics			Forward Dynamics		
	PTM	RTM	FTM	PTM	RTM	FTM
0-150s	**836**	+16.19%	+22.63%	**1110**	+14.90%	+19.42%
150-300s	**540**	+15.08%	+21.37%	**285**	+17.39%	+24.94%

Number of triggering events for PTM (in bold to indicate the best performance) and for RTM and FTM (indicated with percentage increase).

$l_{\mathrm{f}}=2, \boldsymbol{\Gamma}_{\mathrm{v}}^{w}=\boldsymbol{I}_{20}, \boldsymbol{\Gamma}_{\mathrm{f}}^{w}=\boldsymbol{I}_{10}, \boldsymbol{\Gamma}_{\mathrm{v}}^{\epsilon}=0.5\,\boldsymbol{I}_{4}, \boldsymbol{\Gamma}_{\mathrm{f}}^{\epsilon}=0.5\,\boldsymbol{I}_{2}, \sigma_{\mathrm{v}}^{w}=\sigma_{\mathrm{f}}^{w}=0.5$, $\sigma_{\mathrm{v}}^{\epsilon}=\sigma_{\mathrm{f}}^{\epsilon}=0.25$, $\tau_{\mathrm{v}}=\tau_{\mathrm{f}}=0.5$, $\mathcal{O}_{\mathrm{v}}=\mathcal{O}_{\mathrm{f}}=0.75$, $c_{\mathrm{v}}^{1}=c_{\mathrm{f}}^{1}=0.1$, $c_{\mathrm{v}}^{0}=c_{\mathrm{f}}^{0}=0.01$, $\lambda_1=8$, $\lambda_2=12$, $\lambda_3=6$, and $\lambda_{\mathrm{f}}=0.1$.

A. Scenario 1: Different Initial Conditions

In order to show the robustness of our proposed control scheme, this scenario presents the simulation tests by taking the following two sets of initial tracking errors.

1) *Case 1:* Large initial tracking errors: This can be done by selecting initial tracking errors $s_{\mathrm{v},1}(0)=16.87, s_{\mathrm{f},1}(0)=-9.75, s_{\mathrm{v},2}(0)=8.13, s_{\mathrm{f},2}(0)=20.75, s_{\mathrm{v},3}(0)=-11.87$, and $s_{\mathrm{f},3}(0)=-5.25$, and the initial states $h_1(0)=85\,960$ ft, $x_1(0)=369$ ft, $h_2(0)=85\,870$ ft, $x_2(0)=512$ ft, $h_3(0)=85\,660$ ft, and $x_3(0)=226$ ft.
2) *Case 2:* Larger initial tracking errors: This can be done by selecting initial tracking errors $s_{\mathrm{v},1}(0)=-33.13, s_{\mathrm{f},1}(0)=-59.75, s_{\mathrm{v},2}(0)=-41.87, s_{\mathrm{f},2}(0)=120.75, s_{\mathrm{v},3}(0)=-111.87$, and $s_{\mathrm{f},3}(0)=-105.25$, and the initial states $h_1(0)=85\,910$ ft, $x_1(0)=319$ ft, $h_2(0)=85\,820$ ft, $x_2(0)=612$ ft, $h_3(0)=85\,560$ ft, and $x_3(0)=126$ ft.

The results are shown in Figs. 3–6. Fig. 3 indicates that the tracking errors $\boldsymbol{s}_{\mathrm{v},i}\triangleq[s_{\mathrm{v},1},s_{\mathrm{v},2},s_{\mathrm{v},3}]^{\top}=\boldsymbol{h}_{\mathrm{f}}+\boldsymbol{\mathcal{L}}_1^{-1}\boldsymbol{\mathcal{L}}_2\boldsymbol{h}_l$ and $\boldsymbol{s}_{\mathrm{f},i}\triangleq[s_{\mathrm{f},1},s_{\mathrm{f},2},s_{\mathrm{f},3}]^{\top}=\boldsymbol{x}_{\mathrm{f}}+\boldsymbol{\mathcal{L}}_1^{-1}\boldsymbol{\mathcal{L}}_2\boldsymbol{x}_l$, $i\in\{1,2,3\}$ converge to neighborhoods of zero in a rapid manner for all initial tracking errors. Fig. 4 shows that the rigid-body states, control inputs, and sliding mode errors are bounded, especially, Fig. 4(c) and (d) imply that our proposed method not only satisfies actuator constraints but also displays a smooth response. Fig. 5 depicts the position snapshots of all HFVs at five different time instants, from which it can be seen that all follower HFVs converge into the convex hull formed by the leader HFVs, while the leaders achieve the desired formation shape. Fig. 6 displays the trajectories of sampling errors and corresponding dynamic thresholds.

B. Scenario 2: Different Methods

To highlight the superiorities of our proposed triggering mechanism (PTM), comparisons with relative-threshold triggering mechanism (RTM) [20] and the fixed-threshold triggering mechanism (FTM) [27] are provided. The triggering functions in RTM are set as $t_{k_i+1}^{i}=\inf\{t\in\mathbb{R}^{+}|\,||\check{\boldsymbol{e}}_{\mathrm{v},i}(t)||\geq 0.13||\boldsymbol{e}_{\mathrm{v},i}(t)||+0.01\}$ and $t_{k_i+1}^{\mathrm{f},i}=\inf\{t\in\mathbb{R}^{+}|\,||\check{\boldsymbol{e}}_{\mathrm{f},i}(t)||\geq 0.13||\boldsymbol{e}_{\mathrm{f},i}(t)||+0.0001\}$, and the triggering functions in FTM are set as $t_{k_i+1}^{i}=\inf\{t\in\mathbb{R}^{+}|\,||\check{\boldsymbol{e}}_{\mathrm{v},i}(t)||\geq 0.01\}$ and $t_{k_i+1}^{\mathrm{f},i}=\inf\{t\in\mathbb{R}^{+}|\,||\check{\boldsymbol{e}}_{\mathrm{f},i}(t)||\geq 0.0001\}$. The total number event-triggering times of the three methods are shown in Fig. 7 and Table II. It can be seen that the interexecution time of PTM is larger than that of RTM and FTM. In addition, the tracking performances under the three methods are quantified via several performance indices: integral absolute error (IAE) $[\int_0^T|e(t)|\mathrm{d}t]$,

TABLE III
PERFORMANCE INDICES OF THE EXAMINED METHODS

	Vertical Dynamics			Forward Dynamics		
	PTM	RTM	FTM	PTM	RTM	FTM
IAE	**237.84**	285.70	260.42	**107.53**	122.18	114.82
ITAE	**4860.42**	5912.85	5329.03	**2068.13**	2755.09	2540.74
RMSE	**0.51**	0.53	0.53	**0.26**	0.28	0.28

Performance Indices for PTM (in bold to indicate the best performance) and for RTM and FTM.

integral time absolute error (ITAE) $[\int_0^T t|e(t)|\mathrm{d}t]$, root mean square error (RMSE), and $[\frac{1}{T}\int_0^T e^2(t)\mathrm{d}t]^{\frac{1}{2}}$, where e represents the tracking errors $s_{\mathrm{v},i}$ and $s_{\mathrm{f},i}$. The calculation results are summarized in Table III, from which it can be concluded that the performance indices of PTM are smaller than those of RTM and FTM. This means that the PTM not only reduces the communication burden but also guarantees improved tracking accuracy.

VII. CONCLUSION

This article tackled the event-triggered formation-containment control problem for HFV swarm systems with model uncertainties, external disturbances, and actuator dynamics. The proposed protocol guarantees formation-containment control, which means that the follower HFVs converge into a convex hull spanned by multiple leader HFVs, while the leader HFVs maintain a geometric space configuration. Note that the communication network in the current work is fixed: It could be of interest to increase flexibility by considering switchingx topologies. Also, it could be of interest to construct a self-triggered mechanism for further reducing communication resources.

REFERENCES

[1] J. Parker, A. Serrani, S. Yurkovich, M. Bolender, and D. Doman, "Control-oriented modeling of an air-breathing hypersonic vehicle," *J. Guid., Control, Dyn.*, vol. 30, no. 3, pp. 856–869, May 2007.

[2] T. Han, Q. Hu, H. Shin, and M. Xin, "Incremental twisting fault tolerant control for hypersonic vehicles with partial model knowledge," *IEEE Trans. Ind. Informat.*, vol. 18, no. 2, pp. 1050–1060, Feb. 2022.

[3] Y. Zhang, X. Wang, and S. Tang, "A globally fixed-time solution of distributed formation control for multiple hypersonic gliding vehicles," *Aerosp. Sci. Technol.*, vol. 98, Mar. 2020, Art. no. 105643.

[4] Z. Li, B. He, M. Wang, H. Lin, and X. An, "Time-coordination entry guidance for multi-hypersonic vehicles," *Aerosp. Sci. Technol.*, vol. 89, pp. 123–135, Jun. 2019.

[5] Z. Liang, J. Yu, Z. Ren, and Q. Li, "Trajectory planning for cooperative flight of two hypersonic entry vehicles," in *Proc. 21st AIAA Int. Space Planes Hypersonics Technol. Conf.*, 2017, pp. 1–14.

[6] M. Basin, P. Yu, and Y. Shtessel, "Hypersonic missile adaptive sliding mode control using finite- and fixed-time observers," *IEEE Trans. Ind. Electron.*, vol. 65, no. 1, pp. 930–941, Jan. 2018.

[7] J. Sun, Z. Pu, J. Yi, and Z. Liu, "Fixed-time control with uncertainty and measurement noise suppression for hypersonic vehicles via augmented sliding mode observers," *IEEE Trans. Ind. Informat.*, vol. 16, no. 2, pp. 1192–1203, Feb. 2020.

[8] X. Bu, "Air-breathing hypersonic vehicles funnel control using neural approximation of non-affine dynamics," *IEEE/ASME Trans. Mechatronics*, vol. 23, no. 5, pp. 2099–2108, Oct. 2018.

[9] B. Xu, D. Wang, Y. Zhang, and Z. Shi, "DOB-based neural control of flexible hypersonic flight vehicle considering wind effects," *IEEE Trans. Ind. Electron.*, vol. 64, no. 11, pp. 8676–8685, Nov. 2017.

[10] L. Ye, Q. Zong, L. Crassidis, and B. Tian, "Output-redefinition-based dynamic inversion control for a nonminimum phase hypersonic vehicle," *IEEE Trans. Ind. Electron.*, vol. 65, no. 4, pp. 3447–3457, Apr. 2018.

[11] M. Lv, Y. Li, W. Pan, and S. Baldi, "Finite-time fuzzy adaptive constrained tracking control for hypersonic flight vehicles with singularity free switching," *IEEE/ASME Trans. Mechatronics*, to be published, doi: 10.1109/TMECH.2021.3090509.

[12] X. Zhang, Q. Zong, L. Dou, B. Tian, and W. Liu, "Improved finite-time command filtered backstepping fault-tolerant control for flexible hypersonic vehicle," *J. Franklin Inst.*, vol. 357, pp. 8543–8565, 2020.

[13] J. Park, S. Kim, and C. Moon, "Adaptive neural control for strict-feedback nonlinear systems without backstepping," *IEEE Trans. Neural Netw. Learn. Syst.*, vol. 20, no. 7, pp. 1204–1209, Jul. 2009.

[14] M. Ji, G. Ferrari-Trecate, M. Egerstedt, and A. Buffa, "Containment control in mobile networks," *IEEE Trans. Autom. Control*, vol. 53, no. 8, pp. 1972–1975, Sep. 2008.

[15] X. Dong, Y. Hua, Y. Zhou, Z. Ren, and Y. Zhong, "Theory and experiment on formation-containment control of multiple multirotor unmanned aerial vehicle systems," *IEEE Trans. Automat. Sci. Eng.*, vol. 16, no. 1, pp. 229–240, Jan. 2019.

[16] Y. Cao, D. Stuart, W. Ren, and Z. Meng, "Distributed containment control for multiple autonomous vehicles with double-integrator dynamics: Algorithms and experiments," *IEEE Trans. Control Syst. Technol.*, vol. 19, no. 4, pp. 929–938, Jul. 2011.

[17] S. Yoo, "Distributed adaptive containment control of uncertain nonlinear multi-agent systems in strict-feedback form," *Automatica*, vol. 49, no. 7, pp. 2145–2153, Jul. 2013.

[18] X. Dong and G. Hu, "Time-varying formation control for general linear multi-agent systems with switching directed topologies," *Automatica*, vol. 73, pp. 47–55, Sep. 2016.

[19] X. Ge and Q. Han, "Distributed formation control of networked multi-agent systems using a dynamic event-triggered communication mechanism," *IEEE Trans. Ind. Electron.*, vol. 64, no. 10, pp. 8118–8127, Oct. 2017.

[20] L. Xing, C. Wen, Z. Liu, H. Su, and J. Cai, "Event-triggered adaptive control for a class of uncertain nonlinear systems," *IEEE Trans. Autom. Control*, vol. 62, no. 4, pp. 2071–2076, Apr. 2017.

[21] Q. Hu, Y. Shi, and C. Wang, "Event-based formation coordinated control for multiple spacecraft under communication constraints," *IEEE Trans. Syst., Man, Cybern., Syst.*, vol. 51, no. 5, pp. 3168–3179, May 2021.

[22] L. Xing, C. Wen, Z. Liu, H. Su, and J. Cai, "Event-triggered output feedback control for a class of uncertain nonlinear systems," *IEEE Trans. Autom. Control*, vol. 64, no. 1, pp. 290–297, Jan. 2019.

[23] X. Wang, Z. Fei, H. Yan,, and Y. Xu, "Dynamic event-triggered fault detection via zonotopic residual evaluation and its application to vehicle lateral dynamics," *IEEE Trans. Ind. Informat.*, vol. 16, no. 11, pp. 6952–6961, Nov. 2020.

[24] P. S. Berner and M. Monnigmann, "A complexity analysis of event-triggered model predictive control on industrial hardware," *IEEE Trans. Control Syst. Technol.*, vol. 28, no. 6, pp. 2625–2632, Nov. 2020.

[25] C. Wang, L. Guo, C. Wen, X. Yu,, and J. Huang, "Attitude coordination control for spacecraft with disturbances and event-triggered communication," *IEEE Trans. Aerosp. Electron. Syst.*, vol. 57, no. 1, pp. 586–596, Feb. 2021.

[26] W. Wang, S. Tong, and D. Wang, "Adaptive fuzzy containment control of nonlinear systems with unmeasurable states," *IEEE Trans. Cybern.*, vol. 49, no. 3, pp. 961–973, Mar. 2019.

[27] W. Wang, C. Wen, J. Huang, and J. Zhou, "Adaptive consensus of uncertain nonlinear systems with event-triggered communication and intermittent actuator faults," *Automatica*, vol. 111, Jan. 2020, Art. no. 108667.

[28] Z. Liu, X. Tan, R. Yuan, G. Fan, and J. Yi, "Immersion and invariance-based output feedback control of air-breathing hypersonic vehicles," *IEEE Trans. Automat. Sci. Eng.*, vol. 13, no. 1, pp. 394–402, Jan. 2016.

[29] J. Sun, J. Yi, Z. Pu, and Z. Liu, "Adaptive fuzzy nonsmooth backstepping output-feedback control for hypersonic vehicles with finite-time convergence," *IEEE Trans. Fuzzy Syst.*, vol. 28, no. 10, pp. 2320–2334, Oct. 2020.

[30] L. Fiorentini, A. Serrani, M. A. Bolender, and D. B. Doman, "Nonlinear robust adaptive control of flexible air-breathing hypersonic vehicles," *J. Guid., Control, Dyn.*, vol. 32, no. 2, pp. 401–416, Mar. 2009.

Maolong Lv received the B.Sc. and M.Sc. degrees in control science and engineering from Air Force Engineering University, Xi'an, China, in 2014 and 2016 respectively, and the Ph.D. degree in systems and control from the Delft Center for Systems and Control, Delft University of Technology, Delft, The Netherlands, in 2021.

He is currently with the College of Air Traffic Control and Navigation, Air Force Engineering University. His research interests include adaptive learning control, distributed control, reinforcement learning, and intelligent decision-making with applications in multiagent systems, hypersonic vehicles, and unmanned autonomous systems.

Dr. Lv was awarded a Descartes Excellence Fellowship from the French Government in 2018, which allowed him a research visit from 2018 to 2019 at University of Grenoble working on adaptive networked systems with emphasis on traffic with human driven and autonomous vehicles.

Bart De Schutter (Fellow, IEEE) received the Ph.D. (*summa cum laude*) degree in applied sciences from Katholieke Universiteit (KU), Leuven, Belgium, in 1996.

He is currently a Full Professor and Department Head with the Delft Center for Systems and Control, Delft University of Technology, Delft, The Netherlands. He is the coauthor of three books, *Optimal Trajectory Planning and Train Scheduling for Urban Rail Transit Systems*, *Reinforcement Learning and Dynamic Programming Using Function Approximators*, and *Stability Analysis and Nonlinear Observer Design Using Takagi-Sugeno Fuzzy Models* and of more than 200 papers in international journals.

Dr. De Schutter was an Associate Editor for *Automatica* from 2004 to 2016 and is currently an Associate Editor for IEEE TRANSACTIONS ON AUTOMATIC CONTROL and a Senior Editor for IEEE TRANSACTIONS ON INTELLIGENT TRANSPORTATION SYSTEMS.

Simone Baldi (Senior Member, IEEE) received the B.Sc. degree in electrical engineering and the M.Sc. and Ph.D. degrees in automatic control engineering from the University of Florence, Florence, Italy, in 2005, 2007, and 2011, respectively.

He is currently a Professor with the School of Mathematics, Southeast University, Nanjing, China, with guest position at the Delft Center for Systems and Control, TU Delft, Delft, The Netherlands, where he was an Assistant Professor. His research interests include adaptive and switched systems with applications in networked and multiagent control.

Dr. Baldi was the recipient of the Outstanding Reviewer Award for *Automatica* for 2017. He is a Subject Editor for *International Journal of Adaptive Control and Signal Processing* and an Associate Editor for *IEEE Control Systems Letters*.